Master's Thesis

Numerical Investigation of Bubble Movement in Magnetic Nanofluids

Dongkook Joo

Department of Mechanical Engineering

Graduate School of UNIST

2017

Numerical Investigation of Bubble Movement in Magnetic Nanofluids

Dongkook Joo

Department of Mechanical Engineering

Graduate School of UNIST

Numerical Investigation of Bubble Movement in Magnetic Nanofluids

A thesis/dissertation

submitted to the Graduate School of UNIST

in partial fulfillment of the

requirements for the degree of

Master of Science

Dongkook Joo

01. 06. 2017 Month/Day/Year of submission

Approved by

_____

Advisor

Jaeseon Lee

Numerical Investigation of Bubble Movement in Magnetic Nanofluids

Dongkook Joo

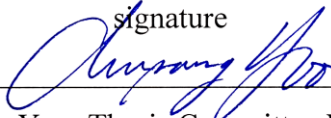This certifies that the thesis/dissertation of Dongkook Joo is approved.

01. 06. 2017 Month/Day/Year of submission

signature

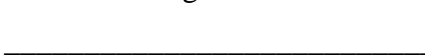_____

Advisor: Jaeseon Lee

signature

_____

Chun Sang Yoo: Thesis Committee Member #1

signature

_____

Jae Hwa Lee: Thesis Committee Member #2

signature

_____

typed name: Thesis Committee Member #3

signature

_____

typed name: Thesis Committee Member #4;

three signatures total in case of masters

Abstract

In this study, the idea to generate electrical energy by using waste heat is suggested. In this idea, the electrical energy can be generated by a magnetic nanofluid and bubble movement. Thus, bubble movement in a magnetic fluid is numerically investigated using the commercial CFD package COMSOL Multiphysics for effective energy generation. The slug characteristics are also investigated because it can be generated by merging each bubble. The level-set method and phase-field method are used to simulate the bubble and slug movement, respectively. For the investigation, EFH1 and EFH3 are selected as working fluids; they are commercial magnetic fluids manufactured by Ferrotec, and each fluid contains different amounts of magnetic particles. The solvers are validated by comparing the numerical results with previous research studies and experimental data for reliable results.

The properties of a fluid can be changed by solid particles if the particles are dispersed in the fluid. These particles can affect the bubble and slug characteristics, such as shape, velocity and wake. Thus, the effect of solid particles is first studied by observing the bubble and slug movement in each magnetic fluid. In the slug investigation, the effects of some parameters are also studied, such as slug length and liquid backflow. The patterns of bubble and slug movement are investigated to predict the effective condition for the energy generation. The effective bubble and slug movements are predicted by evaluating the disturbance of the surrounding magnetic fluid for each flow pattern.

A magnetic force can be created, and it can affect any phenomena when the magnetic field is applied to the system. Thus, the effect of the magnetic force is also investigated because the magnetic field should be applied to the system for the electrical energy generation. Finally, the important factor for energy generation is identified by comparing the results

Contents

List of Figures

List of tables

Nomenclature

Symbol		Unit
U	Rising velocity of bubble and slug	$[m/s]$
d	Diameter of bubble	$[m]$
g	Gravity acceleration	$[m/s^2]$
h	Height of fluid domain	$[m]$
w	Width of fluid domain	$[m]$
F	External force per unit volume	$[N/m^3]$
m	Mass	$[kg]$
f	External free energy	$[J/m^3]$
D	Diameter of fluid domain	$[m]$
H	Strength of magnetic field	$[A/m]$

Greek

ρ	Density	$[kg/m^3]$
μ	Dynamic viscosity	$[Pa \cdot s]$
υ	Kinematic viscosity	$[m^2/s]$
σ	Surface tension	$[N/m]$
ϕ_{ls}	Level-set variable	$[m]$
γ_{ls}	Re-initialization parameter	$[m/s]$
ϵ_{ls}	Interface thickness controlling parameter	$[m]$
ϕ_{pf}	Phase-field variable	$[-]$
ξ	Mobility tuning parameter	$[m \cdot s/kg]$

ϵ_{pf}	Interface thickness controlling parameter	$[m]$
η	Magnetic permeability	$[H/m]$
η_0	Magnetic permeability of vacuum	$[H/m]$
η_r	Relative magnetic permeability	$[-]$
χ	Magnetic susceptibility	$[-]$

Subscript

l	Liquid phase
g	Gas phase
m	Magnetic
t	Total

1. Introduction

In recent years, large amounts of heat energy have been wasted by many power plant systems. However, the energy resources, such as oil and coal, are gradually exhausted. The energy resources can be saved if we reuse the waste heat energy. Thus, in this study, the idea is suggested to generate electrical energy by using the waste heat, as detailed below.
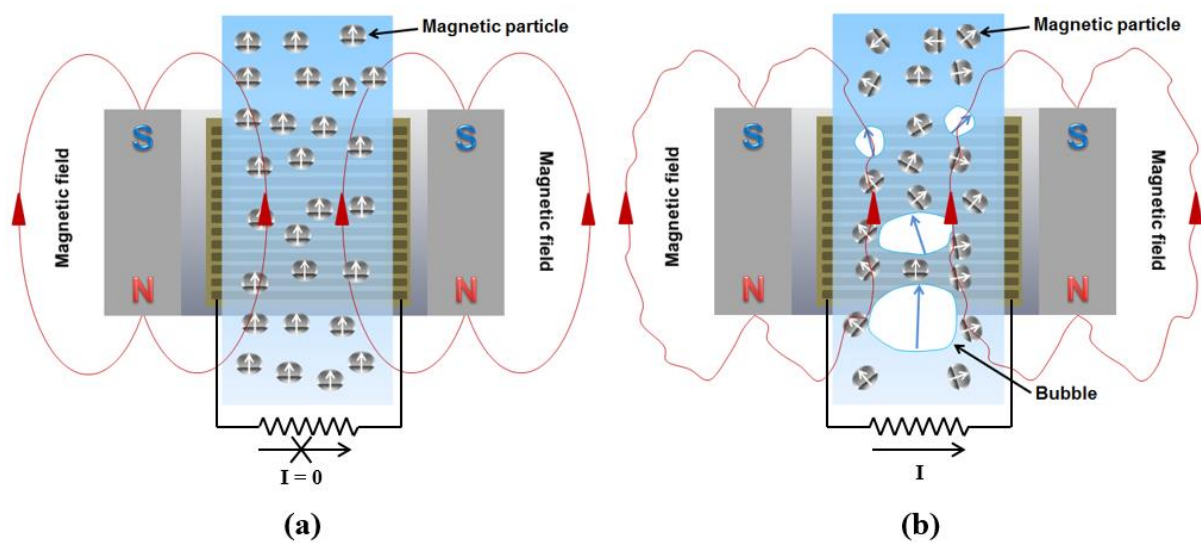
Figure 1.1. Principle of electrical energy generation. (a) w/o bubble, (b) w/ bubble

Figure 1.1 represents the principle of electrical energy generation. When the magnetic nanofluid is placed in the magnetic field, the magnetic particles are aligned by the magnetic field, as shown in figure 1.1-(a). In this state, electrical energy cannot be generated. However, if some of the bubbles move into the magnetic fluid, the magnetic particles can be moved by the bubble movement, and the magnetic field can be disturbed by the motion of the magnetic particles. Finally, the electrical energy can be generated by Faraday's law, as in figure 1.1-(b). In this idea, if the base fluid of the magnetic nanofluid is oil and the bubbles are steam generated by the boiling of water, the steam bubbles only disturb the magnetic particles and leave the magnetic fluid alone because the oil and water cannot be mixed with each other. In addition, the waste heat can be reused as electrical energy if the boiling that is used to generate the bubbles is itself driven by the waste heat. Thus, in this work, the bubble

movement in magnetic nanofluids is numerically investigated to generate electrical energy effectively.

First, understanding of gas bubble characteristics is essential to investigate this situation. In many engineering parts, gas bubbles can be easily observed, such as a vessel, power plant system and medical instrument, and they can affect the performance of the system. Because of this reason, the investigation of bubble characteristics is important and has been studied by many researchers. D. Bhaga and M. E. Weber observed the shape of bubbles, terminal velocity, and flow field around a rising bubble by a hydrogen bubble tracer technique in 1979 [1]. C.W. Stewart investigated the bubble interaction in low–viscosity liquids via experiments in 1994 [2]. K. Tsuchiya, K. Ohsaki and K. Taguchi researched the bubble-bubble interaction patterns for small and large bubbles via experiments in 1994 [3]. R. Krishna and J. M. van Baten investigated the rising characteristics of gas bubbles in a 2D rectangular column by the VOF method in 1997 [4]. In their research, they introduced the VOF method and simulated the rising bubbles according to different bubble and column diameters (distance from the wall). After that, they observed the rising trajectories of bubbles, horizontal movement, rising velocity and bubble-bubble interactions in swarms about each bubble diameter. In their conclusion, they said that the characteristics of bubbles are considerably affected by the bubble diameter and the distance from the wall. Zhao Yu and Liang-Shih Fan investigated the buoyant rise of bubbles in infinite liquid by level-set simulation in 2008 [8]. In their paper, they simulated many cases with different dimensionless numbers and observed the shape, velocity and streamline. In 2015, K dilleswara Rao, M. Vasukiran, A.R.K. Gollakota, Nanda Kishore simulated buoyancy-driven bubbles in milli/micro-channels filled with nanofluid by the level-set method [10]. The characteristics of bubbles have been studied in this manner for a long time by many researchers with different conditions, and the results can be affected by various parameters, such as the fluid properties (density, viscosity, and surface tension), bubble size, distance between each bubble and the wall, etc.

When numerous gas bubbles move in any liquid, they can become larger by merging with each other. Finally, they become a very large bubble, and this large bubble can be a bullet shape because of the wall and its motion, as in figure 1.2.
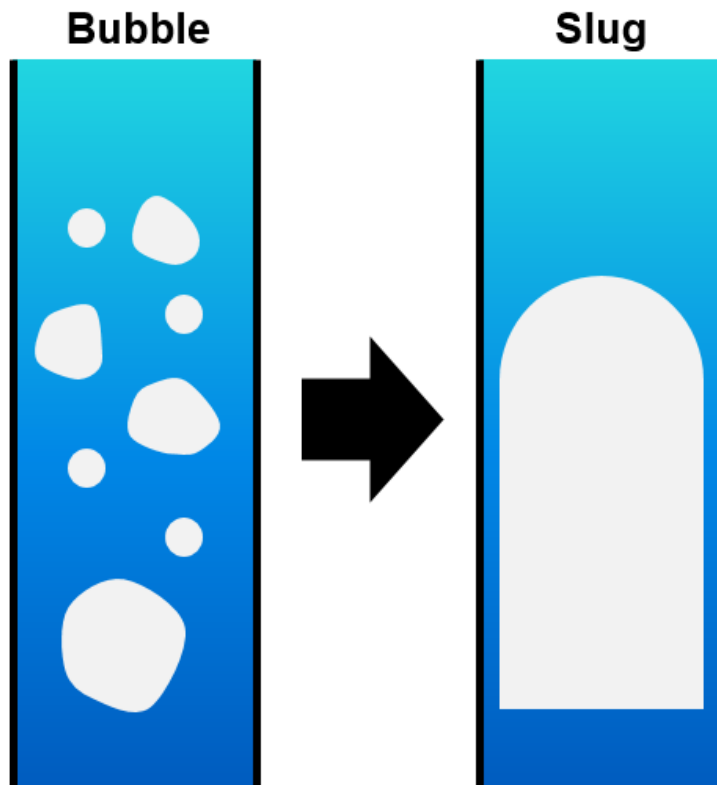
Figure 1.2. Generation of the slug

This bullet-shaped bubble can be called a 'Taylor bubble' or 'Slug.' The characteristics of a slug are slightly different from bubble characteristics. Additionally, this slug is important because of its numerous applications, such as fermenters, production and transportation of hydrocarbons, nuclear reactors and power plants. Thus, it has also been studied by many researchers over a long period of time. In 1961, E. T. White and R. H. Beardmore experimentally investigated the rising velocity of the single cylindrical air bubble rising in a variety of liquids contained in vertically mounted tubes sealed at the lower end [11]. Additionally, in 1962, H.L. Goldsmith and S. G. Mason investigated the movement of a single large bubble in closed vertical tubes. They directly observed the flow patterns in both phases, the thickness of the liquid film surrounding the bubbles, and the shape of the bubble ends [12]. In 1988, J. B. L. M. Campos and J. R. F. Guedes De Carvalho experimentally investigated the wake of gas slugs rising in liquids. They investigated the wake of slugs by two experimental techniques. In their research, they said that the wake pattern can be changed according to the domain size, gravity acceleration and kinematic viscosity of the fluid, and the volume of the wake is not affected by slug length. They also said that the length of the wake is increased when the diameter of

3

the tube is increased or the viscosity of the fluid is decreased [13]. In 2005, Taha Taha and Z. F. Cui numerically investigated the slug flow in vertical tubes. In their research, they investigated the shape of the slug, length of the wake, velocity of the slug and wall shear stress. They also validated the solver to simulate the slug flow by comparing the results with previous research studies [14]. In the present work, the numerical solver is validated by a similar method. In this manner, the slug characteristics, such as rising motion and wake, have also been studied by many researchers and can be affected by fluid properties and domain size, etc.

Understanding of nanofluid is also necessary to investigate the bubble movement in magnetic nanofluid. The nanofluid is the liquid that contains the nanosized solid particles. It is a very interesting topic in today's climate because it has the possibility to improve numerous engineering aspects, such as fuel consumption, pressure drop in fluid flow and heat transfer phenomena. However, its characteristics are very complicated because of the nano-sized solid particles. Thus, many researchers have been investigating nanofluid. H. C. brinkman derived the correlation of viscosity of fluid containing the particles from the Einstein equation in 1951 [15]. S. M. Sohel murshed and Nam-Trung Nguyen investigated the interface tension and viscosity of nanofluid according to the temperature difference via experiments in 2008 [16]. Saad Tanvir and Li Qiao investigated the surface tension of DI-water, ethanol and n-decane-based nanofluid fuels containing suspended aluminum (Al), aluminum oxide (Al2O3), boron (B) and multi-wall carbon nanotubes (MWCNTs) using the pendant drop method by solving the Young-Laplace equation in 2012 [17]. In previous research studies, they reported that nanofluid can improve any engineering situation. However, it is still difficult to understand the characteristics of nanofluid clearly. Regarding the properties of nanofluid, the density and viscosity of nanofluid tend to increase with the increase of particle concentration. However, the surface tension changes irregularly according to the type of particle and base fluid. Thus, in this work, the properties of commercial magnetic nanofluid are used for simulation because the properties of nanofluid cannot be calculated directly.

Regarding the energy generation idea, the magnetic field should be applied to the system to generate the electrical energy. Thus, the effect of the magnetic force on the bubble movement should be considered. The fluid phenomena can be changed by the magnetic force when the magnetic field is applied to the fluid domain. Thus, the effect of the magnetic force on the flow field has been studied by various researchers. In 1996, N. I. Wakayama, H. Ito, Y. Kuroda, O. Fujita and K. Ito addressed a simple method of generating convective air flows for the application of magnetic fields and supporting combustion under microgravity conditions [18]. Nobuko I. Wakayama again investigated the magnetic buoyancy force acting on the bubbles in non-conducting and diamagnetic fluids under

4

microgravity [19]. In their research, the authors investigated the effect of magnetic force on gas bubbles under normal and microgravity conditions. The authors stated that the magnetic force acting on the flow field is much smaller than the gravitational force. Thus, it is difficult to observe the clear effect of the magnetic force in normal gravity conditions. However, in microgravity conditions, the observation of the magnetic force effect is possible, and the magnetic force can drive the bubble. In 2000, Jianwei Qi, Nobuko I. Wakayama and Akira Yabe numerically simulated the effect of a vertical magnetic field gradient on thermal convection in paramagnetic fluids [20]. In this manner, various researchers have investigated the magnetic force effect on the flow field and how it can affect the fluid phenomena.

In other words, to generate the electrical energy effectively, the investigation of bubble movement in magnetic nanofluids is necessary. However, as mentioned above, it has not been studied yet. Thus, the bubble movement in magnetic nanofluids is numerically investigated in this work. Additionally, the effect of magnetic force on bubble characteristics is also investigated.

2. Investigation of bubble movement

2.1. Bubble dynamics

When a gas bubble exists in any liquid, it can be driven upward by the buoyancy force (density difference). Then, its characteristics, such as rising velocity and shape, can be determined by three dimensionless numbers: the Eotvos number, Morton number and Reynolds number [1, 8]. These are introduced below.

Reynolds number

$$\text{Re} = \frac{\rho_l U d}{\mu_l} \tag{2-1}$$

Eotvos number

$$\text{Eo} = \frac{(\rho_l - \rho_g) g d^2}{\sigma} \tag{2-2}$$

Morton number

$$\text{Mo} = \frac{g(\rho_l - \rho_g)\mu_l^4}{\rho_l^2 \sigma^3} \tag{2-3}$$

As we can see, each dimensionless number is related to the fluid properties (viscosity, density and surface tension), bubble size, gravity acceleration and bubble rising velocity. From these numbers, D. Bhaga and M. E. Weber experimentally investigated the bubble characteristics with various fluids and introduced the bubble regime diagram, which can comprehensively show the characteristics of a bubble driven by the buoyancy force [1].
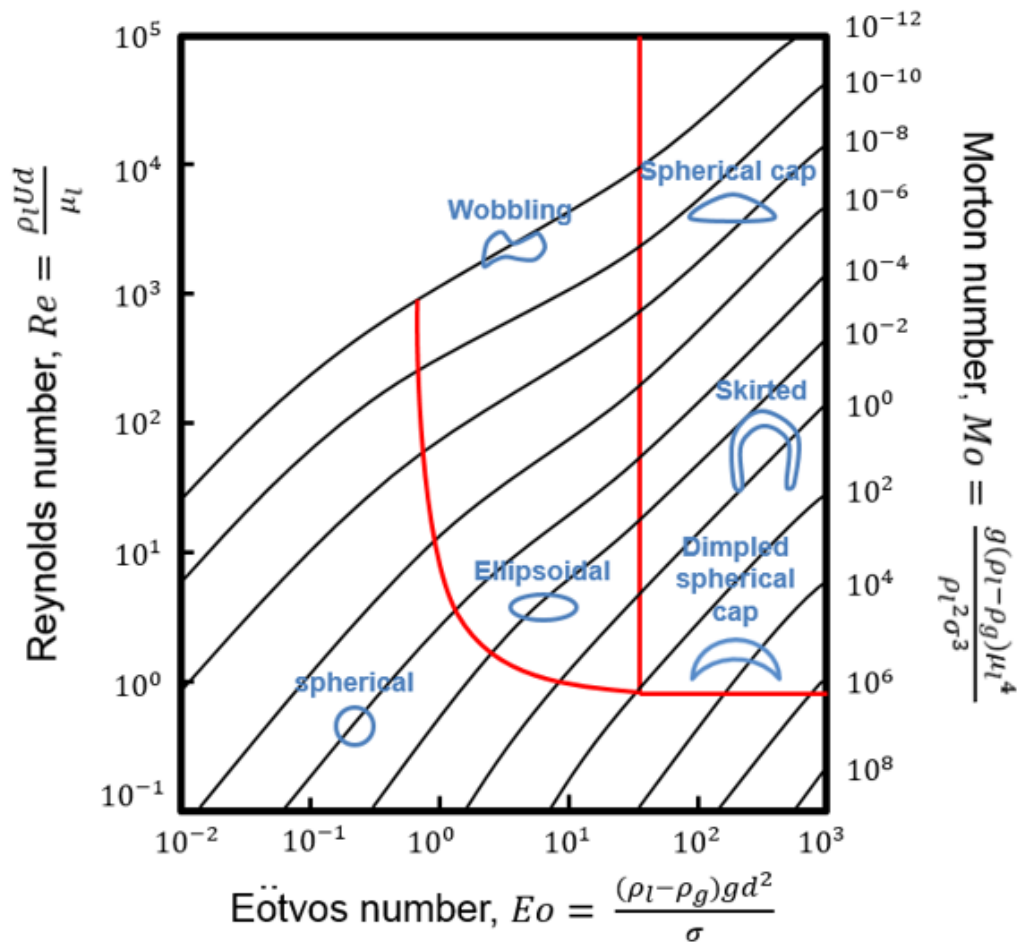
Figure 2.1. Bubble regime diagram

As shown in figure 2.1, the bubble regime diagram represents the bubble shape according to three dimensionless numbers. The bubble can become various shapes according to fluid properties and size. When any gas bubble moves in any liquid, the Eotvos number and Morton number are initially determined by the fluid properties and size. Then, the Reynolds number can be determined by the bubble regime diagram, and the rising velocity can be calculated from the Reynolds number. Finally, the bubble shape can be determined by the bubble regime diagram. In other words, the characteristics such as bubble rising velocity and bubble shape can be predicted by the bubble regime diagram. Thus, the numerical solver used in the present study will be validated by comparing the numerical results with the bubble regime diagram in a later section.

2.2. Level-set method

In this study, the level-set method is used to numerically investigate the bubble movement. The level-set method was devised by Stanley Osher and James Sethian as a simple and versatile method for computing and analyzing the motion of an interface in two or three dimensions. In other words, the level-set method is a technique for representing the moving interface or boundaries using a fixed mesh. This is capable of capturing topological changes and can compute geometric quantities easily. Additionally, it is relatively easy to implement. However, it is computationally expensive, requires re-initialization to maintain the signed distance function, and has a loss or gain of mass due to numerical diffusion. Nevertheless, the level-set method is good for capturing the moving interface.
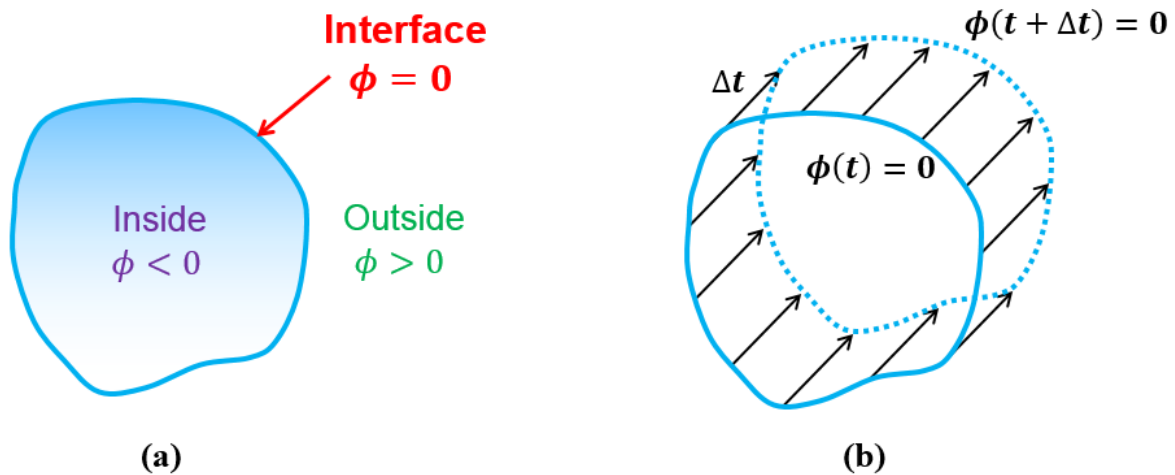
Figure 2.2. Principle of level-set method, (a) Definition of level-set function, (b) Advection of interface

Figure 2.2 shows the principle of the level-set method. To capture the bubble surface via the level-set method, the scalar function is defined (level-set variable, ϕ_{ls}), which is the distance from the bubble surface. Then, the value of the level-set variable is '0' on the bubble surface. Additionally, the level-set variable has a (-) and (+) value at the inside and outside of the bubble, respectively. From the level-set variable, the problem can be recast with one additional dimension ϕ_{ls}, and finally, the bubble surface can be captured by solving the equations. Including the level-set equation, the three equations should be solved to simulate the gas bubble movement in the liquid.

Continuity equation

$$\nabla \cdot u = 0 \tag{2-4}$$

Momentum equation

$$\rho \frac{\partial u}{\partial t} + \rho(u \cdot \nabla)u = \nabla \cdot [-pI + \mu(\nabla u + (\nabla u)^T)] + \rho g + F \tag{2-5}$$

Level-set equation

$$\frac{\partial \phi_{ls}}{\partial t} + \nabla \cdot (u\phi_{ls}) = \gamma_{ls}\nabla \cdot (\epsilon_{ls}\nabla\phi_{ls} - \phi_{ls}(1 - \phi_{ls})\frac{\nabla\phi_{ls}}{|\nabla\phi_{ls}|}) \tag{2-6}$$

The first and second equations are continuity and momentum equations. They are basic and essential equations for investigating the fluid phenomena. On the RHS of the momentum equation, the F term represents an external force that can be additionally generated in any arbitrary situation. Thus, the magnetic force calculation should be put on the RHS of the momentum equation as an additional force for investigating the magnetic force effect in this study.

The third equation is the level-set equation to capture the bubble surface. In the level-set equation, the LHS gives the correct motion of the bubble surface, and the RHS is necessary for numerical stability. On the LHS of the level-set equation, $\nabla \cdot (u\phi_{ls})$ is a convective term and is set with a conservative form to prevent the dissolution of the gas bubble (mass loss). On the RHS of the level-set equation, ϵ_{ls} is the controlling parameter related to the thickness of the bubble surface, and γ_{ls} is the re-initialization parameter. As mentioned above, the level-set method requires the re-initialization to maintain the signed distance function. In this regard, γ_{ls} represents the speed of re-initialization of the level-set function. A suitable value for γ_{ls} is the maximum magnitude of the velocity field. If γ_{ls} is too small, the thickness of the interface might not remain constant, and if γ_{ls} is too large, the interface moves incorrectly. However, the maximum magnitude of the velocity field usually cannot be known before investigating the situation. Thus, the default value of γ_{ls} is used for investigation ($\gamma_{ls} = 1$) in the present study, and it is reasonable for most situations [10, 24]. It will also be

validated in a later section.

2.3. Conditions for simulation

The schematic of the bubble simulation is presented in figure 2.3.
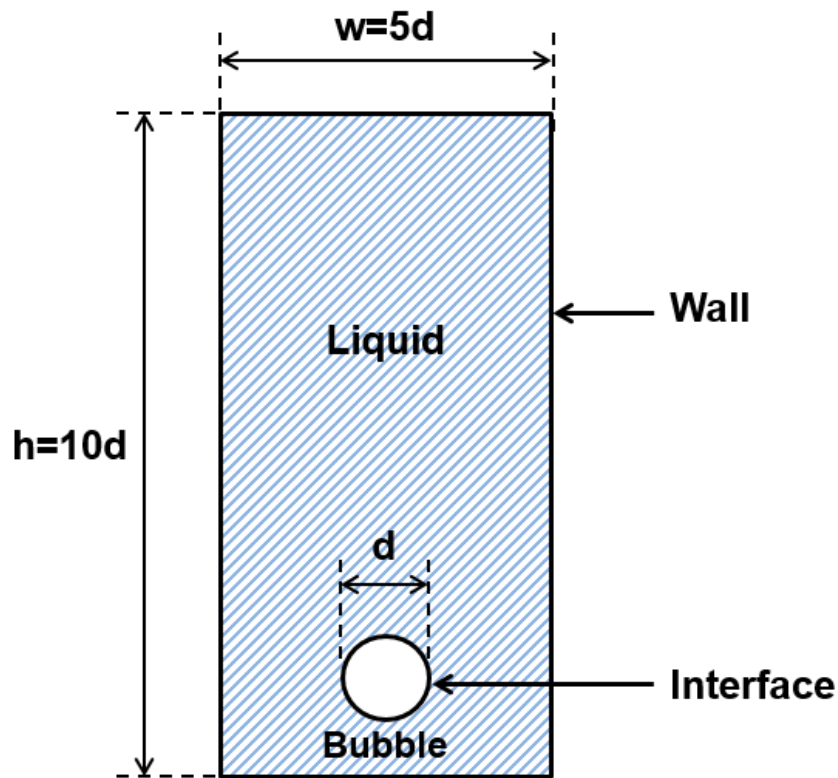
Figure 2.3. Schematic of bubble simulation

In figure 2.3, the flow field is initially filled with any liquid, and the gas bubble is placed in it. All boundaries are treated as no-slip boundary conditions. The width and height of the fluid domain are 5 times and 10 times the bubble diameter, respectively. Additionally, the initial gas-liquid interface (bubble surface) is set as in figure 2.3.

In this study, the steam (water vapor) and oil based magnetic fluids are selected as the gas bubble and surrounding liquid because the bubble and surrounding liquid should not be mixed with each other for

the energy generation. Thus, the properties of each fluid are necessary for the numerical investigation, and the properties of steam can be easily known. As mentioned above, however, the properties of nanofluid cannot be easily known because of its complex characteristics. In particular, the surface tension of nanofluid is changed irregularly according to the type of particle and base fluid. Thus, the EFH1 and EFH3 are considered in the present work; they are commercial magnetic nanofluids manufactured by the Ferrotec company. The physical properties of each magnetic nanofluid are presented in Table 2.1.

Table 2.1. Properties of magnetic nanofluids (EFH 1, EFH 3)

	Carrier liquid	Particle	Particle size (diameter)	Particle concentration (Vol%)	Density [kg/m3]	Viscosity [Pa·s]	Surface Tension [N/m]
EFH 1	Light hydrocarbon oil	Fe3O4	10nm	7.9%	1210	0.006	0.029
EFH 3	Light hydrocarbon oil	Fe3O4	10nm	11.8%	1420	0.012	0.029

The EFH is commercial magnetic nanofluid that consists of light paraffinic hydrocarbon oil and Fe_3O_4 particles. The size of the magnetic particles is 10 nm. The EFH 1 and EFH 3 contain different amounts of particles, 7.9% and 11.8% of the volume concentration, respectively. Thus, each fluid has different values of density and viscosity. However, the surface tension is the same for each fluid. This cannot be explained clearly because the surface tension of nanofluid changes irregularly according to the type of particle and base fluid. However, this value is reliable because it is measured by the manufacturer. Thus, the bubble movement in the magnetic fluid can be simulated from these data.

To investigate the bubble movement, the computational domain is uniformly constructed with fixed triangular meshes in the entire domain, and the number of elements can affect the simulation results as in figure 2.4.
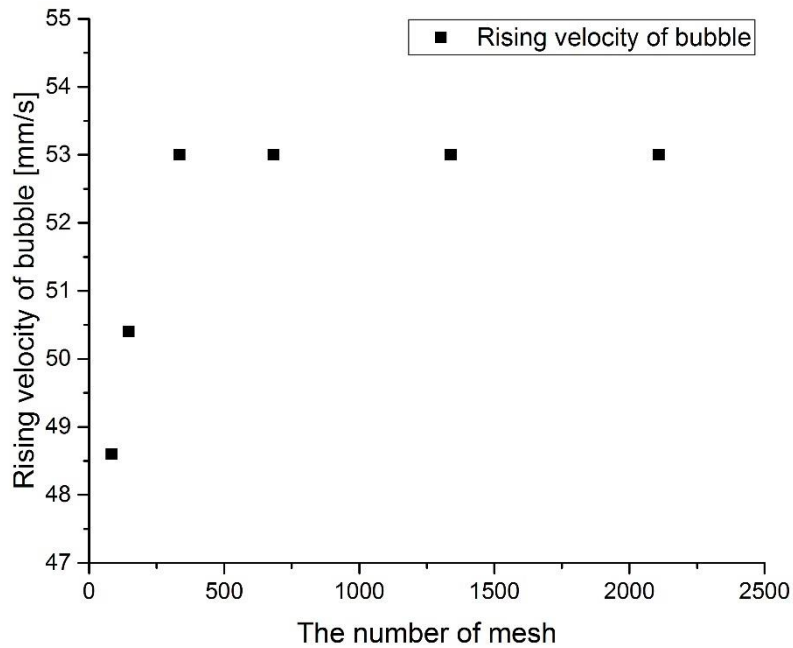
Figure 2.4. Mesh dependency test; Rising velocity of bubble

Figure 2.4 represents the bubble rising velocity according to the number of elements in the bubble cross-sectional area. As we can see, the rising velocity of the bubble is increasing when the number of elements is increasing, and it becomes nearly constant when the number of elements is larger than 335. Thus, the following studies are conducted with more than 335 elements.

2.4. Validation of the solver

In this part, the numerical solver that is used in this study is validated by comparing the numerical results with the bubble regime diagram and experimental data. Additionally, the bubble regime diagram is studied in detail.

2.4.1. Comparison with the bubble regime diagram

As mentioned above, the bubble rising velocity and bubble shape can be predicted by the bubble regime diagram when the gas bubble is driven by the buoyancy force in the liquid. Thus, the solver

can be validated by comparing the numerical results with the bubble regime diagram. To validate the solver for every bubble shape, the simulation is conducted for various cases as described below.

Table 2.2. Simulation cases for solver validation

	$\rho[kg/m^3]$	$\mu[Pa \cdot s]$	d[m]	$\sigma[N/m]$	Eo	Mo	Re	Rising velocity [m/s]	Regime
A1	1000	0.01	0.002	0.01	3.92	9.8E-05	18	0.09	Oblate ellipsoidal
A2	1000	0.01	0.001	0.01	0.98	9.8E-05	5	0.05	Sphere
B1	1000	0.97	0.016	0.022	114.036	814.789	2.034	0.123	Ellipsoidal cap
B2	1000	0.73	0.016	0.022	114.036	261.366	2.991	0.136	Ellipsoidal cap
B3	1000	0.46	0.016	0.022	114.036	41.209	5.214	0.150	Ellipsoidal cap
B4	1000	0.277	0.016	0.022	114.036	5.418	12.448	0.216	Ellipsoidal cap
B5	1000	0.195	0.016	0.022	114.036	1.331	13.538	0.165	Ellipsoidal cap
C	1000	1	0.04	0.072	217.778	26.256	10.1	0.253	Skirted
D	1000	0.046	0.01	0.06	16.333	2.031E-04	28.413	0.131	Ellipsoidal or disk
E	1000	0.001	0.008	0.072	8.711	2.626E-11	1120	0.14	Wobbling
F	1000	0.01	0.008	0.072	8.711	2.626E-07	113.6	0.142	Oscillating or disk
G	1000	0.1	0.04	0.072	217.778	2.626E-03	108	0.27	Spherical cap

Table 2.2 represents the simulation conditions and results (rising velocity and bubble shape) for solver validation. Most of the cases in Table 2.2 are provided by reference [8], and others (A2, G) are additional cases for investigating every bubble shape. These results are represented on the bubble regime diagram for comparison as in figure 2.5.
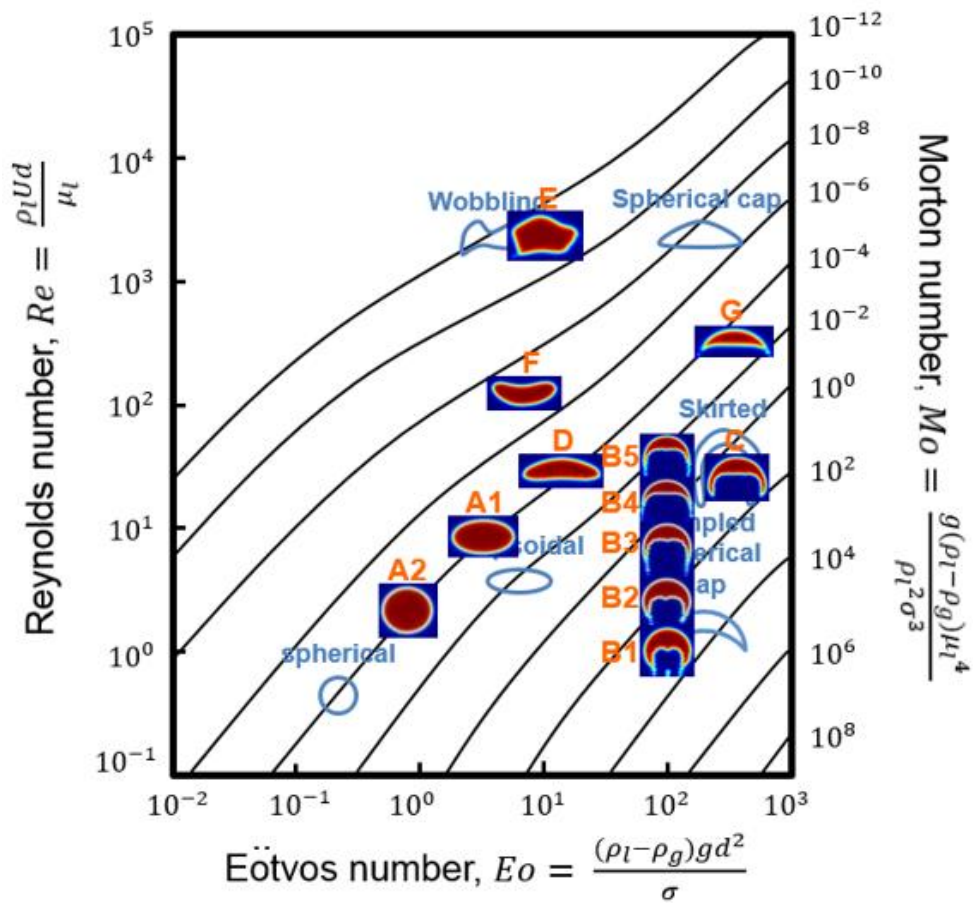
Figure 2.5. Comparison of the results with bubble regime diagram

In figure 2.5, it is easily observed that the numerical results agree well with the bubble regime diagram. Thus, the solver is reliable and can give good results for bubble investigation. For cases A1-A2, they have the same fluid properties, and the bubble diameter is different for each case. The rising velocity and shape are different for each case because of the difference in diameter. Thus, the characteristics of a bubble can be changed by its size even though its properties are the same. For cases B1-B5, the bubble diameter and fluid properties are the same except for the viscosity of fluid. In these cases, only the viscosity is decreasing gradually. Thus, the Eotvos number is the same for each case, and the Morton number is reduced gradually. Thus, its shape is changed from a dimpled ellipsoidal cap to a skirted form, and the characteristics of the bubble can be changed by the viscosity of the fluid. For case G, the bubble shape is a spherical cap, and this is generated in a very interesting manner. Figure 2.6 represents the change of bubble shape for case G.
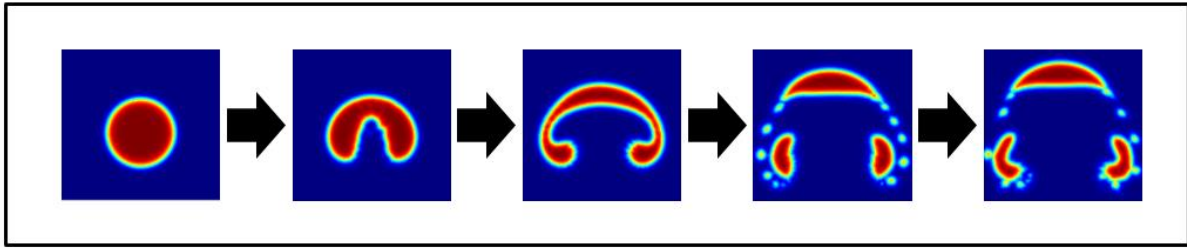
Figure 2.6. Change of bubble shape (Case G; Spherical cap)

In figure 2.6, the bubble shape is initially a sphere (initial set). As time passes, however, the bottom of the bubble is dimpled, and the small part of the bubble reaches to both sides of the bubble. Finally, this small part, which has reached the bubble side, is separated from the bubble body. Through this process, the spherical cap bubble can be generated.

In this part, many types of bubbles are investigated by changing the fluid properties and bubble diameter. In addition, it is observed that the simulation results agree well with the bubble regime diagram. Thus, the solver that is used in this study is reliable for investigating the bubble movement. The default value of γ_{ls} is also validated because all cases are simulated with $\gamma_{ls} = 1$.

2.4.2. Comparison with experimental data

In the present study, the bubble movement is also observed by experiment. Thus, the solver is validated again by comparing the numerical results with experimental results in this part.
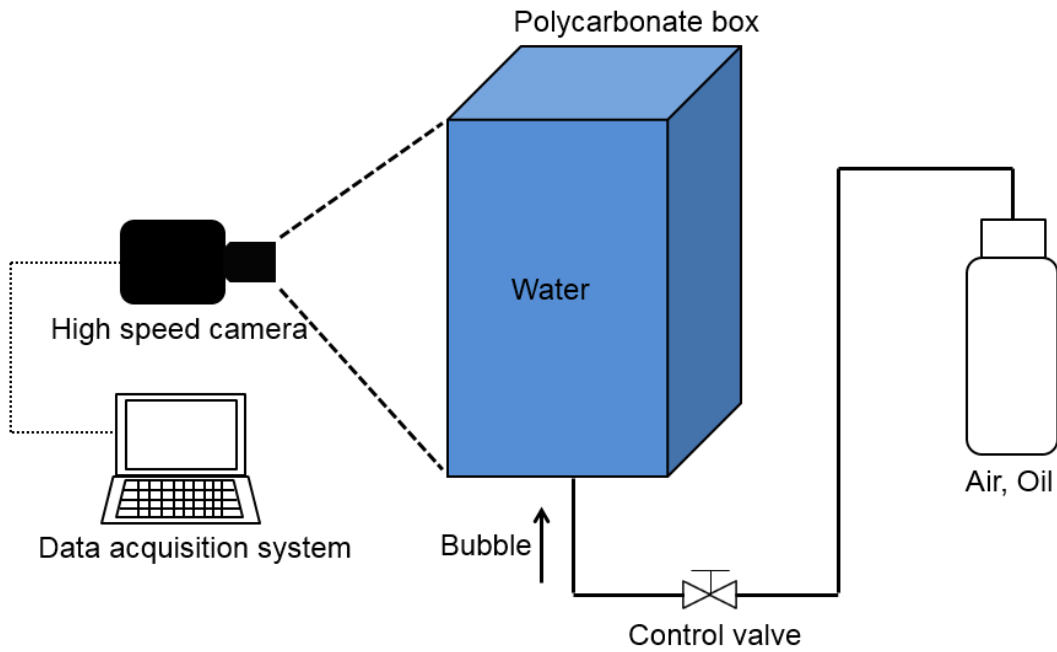
Figure 2.7. Schematic of experimental apparatus (Bubble movement)

Figure 2.7 represents the schematic of the bubble experiment. It consists of a test box, air and oil container, control valve and high-speed camera. The test box is made of polycarbonate and is transparent. Thus, the inside of the box can be observed. This box is initially filled with DI-water; the bubble is injected into the box and can be controlled by the valve. When the bubble moves in the box, its motion and shape can be captured by the high-speed camera. The air and oil bubble movement in DI-water are observed by experiment, and each result is compared with the numerical result.
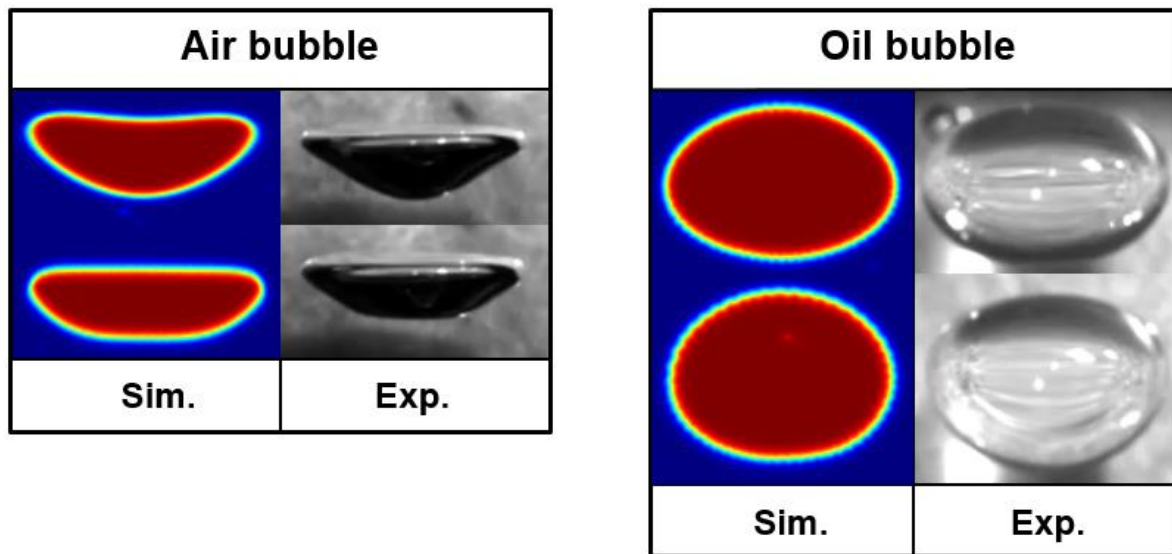
Figure 2.8. Comparison of bubble shape; Simulation vs Experiment

Figure 2.8 shows the shape of the air and oil bubble from simulation and experiment, respectively. The diameter of the air bubble is 5 mm, and that of the oil bubble is 7.5 mm. For the air bubble, the Eotvos number is 3.4, and the Morton number is 2.63E-11. It is located in the wobbling shape zone in the bubble regime diagram. Thus, the bubble shape should be wobbled randomly, and it is well represented by simulation and experiment. The oil bubble is a liquid bubble. Thus, it is not related to the bubble regime diagram. However, it can be easily observed that the shape of the oil bubble is nearly the same in simulation and experiment. Thus, figure 2.8 shows us that the solver can give good results for bubble investigation.

2.5. Results and discussion

2.5.1. Effect of solid particle

In this part, the effect of solid particles is investigated for bubble movement. The EFH1 and EFH3 consist of the same type of base fluid and particles. Only the amount of particles is different for each magnetic fluid. Thus, the effect of solid particles can be observed by comparing the bubble movement in each magnetic fluid. Figure 2.9 represents the motion of a single bubble in EFH1 and EFH3 with different bubble diameters.
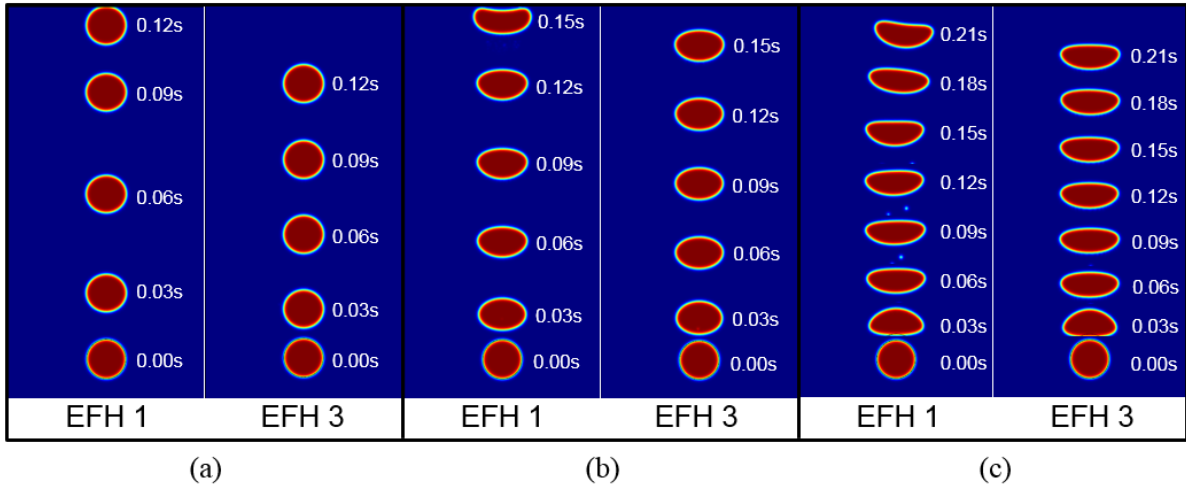
Figure 2.9. Single bubble movement in EFH1 and EFH3;

(a) d=1mm; Eo=0.41, Mo=4.31E-7 for EFH1; Eo=0.48, Mo=5.87E-6 for EFH3

(b) d=2mm; Eo=1.64, Mo=4.31E-7 for EFH1; Eo=1.92, Mo=5.87E-6 for EFH3

(c) d=3mm; Eo=3.68, Mo=4.31E-7 for EFH1; Eo=4.32, Mo=5.87E-6 for EFH3

In figure 2.9, it can be easily observed that the bubble in EFH3 is slower than that in EFH1 regardless of bubble diameter. When the solid particles are dispersed in liquid, the viscosity of the liquid is increased by the additional friction of the solid particles. Thus, higher friction drag can act on the bubble, which moves in EFH3. Because of this, the bubble rises faster in EFH1 than in EFH3. However, the shape of the bubble in each magnetic fluid is nearly the same if the bubble diameter is the same. In figure 2.9-(a), the Eotvos number and Morton number of the 1-mm bubble in EFH1 are 0.41 and 4.31E-7. For the EFH3 case, the Eotvos number and Morton number are 0.48 and 5.87E-6, respectively. In this manner, the same size of bubble in each magnetic fluid has obviously different dimensionless numbers because of the property differences. However, in the bubble regime diagram, both cases are located in the same region (sphere shape). Thus, the bubble shape is nearly the same for each case although the dimensionless numbers are different. It is the same for the 2-mm and 3-mm bubble cases. Thus, the differences in properties between EFH1 and EFH3 do not affect the bubble shape because the property differences are not large enough to change the bubble shape. However, the bubble shape can be changed if a much greater quantity of solid particles are dispersed in the fluid.

18

The interaction of two bubbles is also investigated for each magnetic fluid. Because of different fluid properties, it can be predicted that the bubble-bubble interaction is also different in each magnetic fluid.
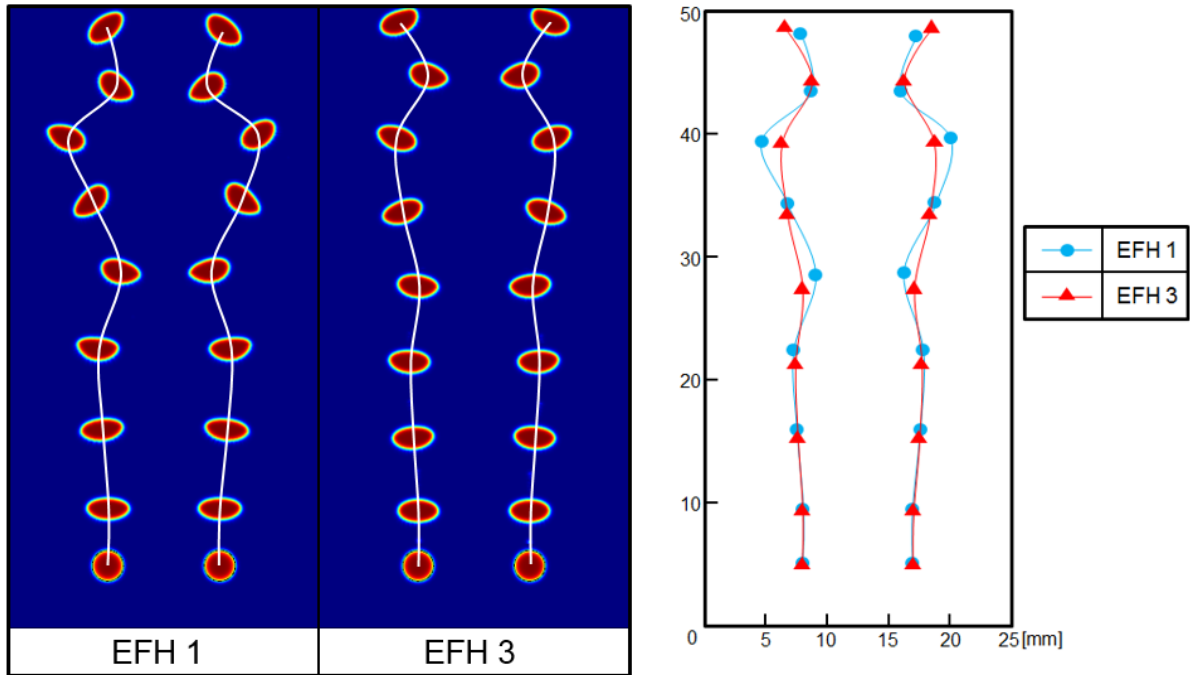
Figure 2.10. Interaction of two bubbles in EFH1 and EFH3

Figure 2.10 represents the interaction of two bubbles in each magnetic nanofluid. In this case, the bubbles rise straight upward initially. As time passes, however, the bubbles fluctuate in the horizontal direction due to the effect of each bubble and the wall. When the bubbles fluctuate due to interaction, the bubbles in EFH1 have a larger amplitude in the horizontal direction than those in EFH3. In other words, the bubbles in EFH1 can move more actively in the horizontal direction by interaction than the bubbles in EFH3. This can also be explained by considering the viscous friction. The EFH3 has higher viscosity than EFH1 due to the additional solid particles, as mentioned above. Thus, the bubble movement in EFH3 is disrupted more strongly than in the EFH1 case. Thus, the bubble in EFH1 can have a larger amplitude than the bubble in EFH3.

In this part, the effect of solid particles is investigated by comparing the simulation results for each magnetic nanofluid. The bubble can move more actively if a smaller amount of solid particles is

dispersed in the liquid. However, the shape of the bubble is nearly the same in each magnetic fluid. These results should be considered when we generate the energy by using the magnetic fluid and bubble movement.

2.5.2. Effective bubble movement for energy generation

In this part, effective bubble movement is predicted to generate greater amounts of electrical energy. First, the patterns of bubble movement are investigated to predict the effective bubble movement. When two bubbles of the same size move in the magnetic fluid (EFH1), they can move via 4 patterns according to the initial distance between each bubble.
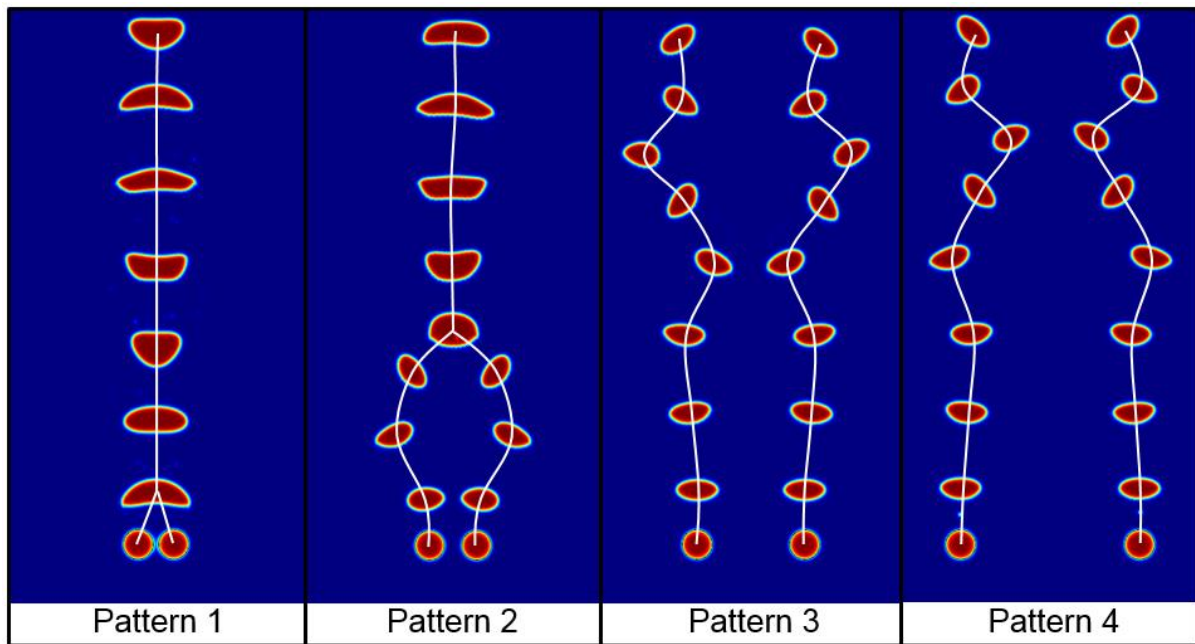
Figure 2.11. Interaction patterns of two bubbles

Figure 2.11 shows the interaction patterns of two bubbles. The first pattern is that the two bubbles are initially merged and move in the magnetic fluid as a big bubble. In pattern 2, the two bubbles initially exhibit fluctuations due to the effect of each bubble and the wall. Next, they merge with each other and move in the liquid as a big bubble. In patterns 3 and 4, the two bubbles move upward with fluctuations due to the effect of each bubble and the wall. However, the direction of fluctuation is

opposite for each pattern. Two bubbles of the same size can move in these 4 patterns, and effective bubble movement is investigated by these movement patterns.
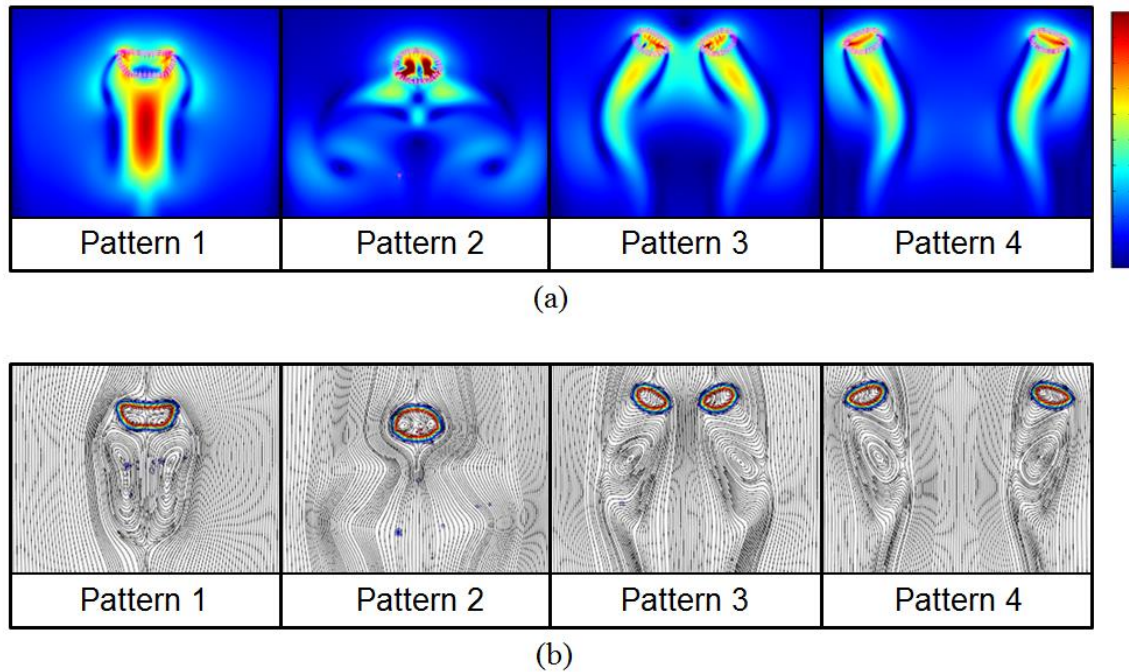
Figure 2.12. (a) Velocity field, (b) Streamline of each pattern at t=0.2s

Figure 2.12 represents the velocity field (a) and streamline (b) of each pattern at 0.2 s. In pattern 1, one big bubble is rising upward with a terminal rising velocity at 0.2 s. In pattern 2, the two bubbles are merged as a big bubble at 0.2 s. In patterns 3 and 4, the two bubbles are rising with fluctuations at 0.2 s. In this manner, each pattern represents its characteristics at 0.2 s. Thus, the effective bubble movement can be predicted by observing each pattern at 0.2 s. In figure 2.12-(a), the surrounding magnetic fluid has a larger velocity magnitude when one big bubble moves in the liquid (pattern 1) than in other cases. This means that the magnetic fluid can be moved faster, that the magnetic field can be disturbed more actively, and finally that a greater amount of energy can be generated by this movement. Additionally, in figure 2.12-(b), the recirculation flow appears over the larger area when one big bubble moves in the liquid (pattern 1) than in other cases. It also means that the surrounding magnetic fluid is more actively mixed in this case. Thus, this case can induce a greater amount of energy generation than others. Thus, it is predicted from figure 2.12 that one large bubble is more

effective than two small bubbles for generating electrical energy. In other words, a large amount of energy may be generated when the large bubble moves in a magnetic fluid.

However, this is just an approximate analysis. For more reliable prediction, the movement of the magnetic fluid should be evaluated by any quantitative value. Thus, the average velocity of only the magnetic fluid is calculated by equation 2-7 for the quantitative analysis.

$$\bar{U}_{liquid} = \frac{\int [(Volume\ fraction\ of\ liquid) \times (Velocity\ magnitude)]\ dA}{\int (Volume\ fraction\ of\ liquid)\ dA} \qquad (2\text{-}7)$$

In the above equation, the denominator represents the integration of the magnetic fluid velocity in the fluid domain. The numerator represents the surface area that is filled with magnetic fluid. Thus, the average velocity of the magnetic fluid can be calculated by equation 2-7, and the movement of the magnetic fluid can be evaluated quantitatively. Finally, the effective bubble movement can be predicted for energy generation.
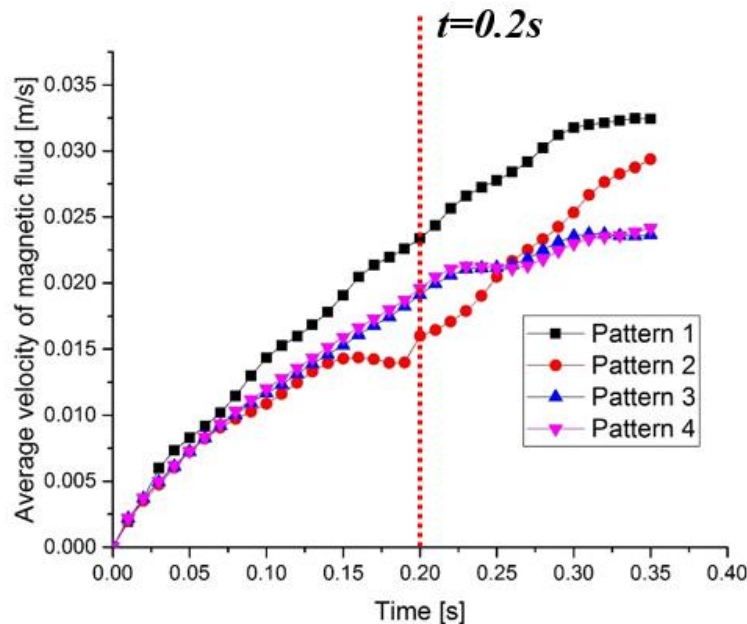

Figure 2.13. Average velocity of surrounding liquid for each pattern

22

Figure 2.13 represents the average velocity of magnetic fluid for each pattern. Initially, the average velocity of magnetic fluid is 0 for every case. As time passes, the velocity of the surrounding magnetic fluid is increased gradually because of the bubble movement. After the rising has begun, the velocity of the magnetic fluid is always higher in pattern 1 than in the others. This means that pattern 1 is most effective for generating the electrical energy. In other words, the big bubble is more effective for generating energy than small bubbles, as we predicted above, because the higher velocity of the magnetic fluid can induce a more active disturbance of the magnetic field.

For patterns 2-4, the velocity of magnetic fluid is higher in patterns 3 and 4 than in pattern 2 during 0.15 s-0.25 s because two small bubbles are merged with each other in pattern 2. When two bubbles are merged, as in pattern 2, the rising velocity is decreased temporarily because they are merged in the horizontal direction. Thus, the velocity of the magnetic fluid is also decreased during this time. However, after merging is finished, the velocity of the magnetic fluid is higher in pattern 2 than in patterns 3 and 4 because the bubble in pattern 2 moves as a big bubble. Thus, it is confirmed that the big bubble is more effective for generating energy than small bubbles. However, the temporary decrease of the magnetic fluid velocity can be induced when the bubbles are merged in the horizontal direction as in pattern 2.

In this part, the effective bubble movement is investigated by observing the velocity field and streamline of magnetic fluid for each interaction pattern. The results show that the big bubble can be more effective for generating electrical energy than a small bubble. It is confirmed by calculating the average velocity of the magnetic fluid

3. Investigation of slug movement

In the energy generation idea, the slug can be generated by merging each bubble. Thus, understanding of slug characteristics is also necessary, and so the slug movement in a magnetic fluid is investigated in this section.

3.1. Phase-field method

In this study, the phase-field method is used to numerically investigate the slug movement. Like the level-set method, the phase-field method is a technique to represent a moving interface or boundaries by defining any scalar function. For the level-set method, the scalar function (level-set variable) is defined as a distance from the interface to track the interface. However, for the phase-field method, the scalar function (phase-field variable, ϕ_{pf}) is related to the mass fraction of the fluid as detailed below.

$$\phi_{pf} = \frac{m_l - m_g}{m_l + m_g} \tag{3-1}$$

In the above definition, the value of the phase-field variable is '0' on the interface. Additionally, the phase-field variables are '-1' and '+1' at the inside and outside of the interface, respectively. The surface of the slug can be captured by using the phase-field variable. For the level-set method, the fluid interface is simply convected with the flow field. However, the phase-field method not only convects the fluid interface but also considers the total free energy for the stability of the system. Thus, the phase-field method includes more physics than the level-set method. For the slug movement, the system can be more unstable than the bubble movement because its scale is higher, and it also includes the relation with wall friction. Thus, the phase-field method is used to investigate the slug movement instead of the level-set method. Like the level-set method, the three equations should be solved to numerically investigate the slug movement, including the phase-field equation.

Continuity equation

$$\nabla \cdot u = 0 \tag{3-2}$$

Momentum equation

$$\rho \frac{\partial u}{\partial t} + \rho(u \cdot \nabla)u = \nabla \cdot [-pI + \mu(\nabla u + (\nabla u)^T)] + \rho g + F \tag{3-3}$$

Phase-field equation

$$\frac{\partial \phi_{pf}}{\partial t} + u \cdot \nabla \phi_{pf} = \nabla \cdot \frac{\gamma_{pf}\lambda}{\epsilon_{pf}^2} \nabla \psi \tag{3-4}$$

$$\left(\psi = -\nabla \cdot \epsilon_{pf}^2 \nabla \phi_{pf} + (\phi_{pf}^2 - 1)\phi_{pf} + \frac{\epsilon_{pf}^2}{\lambda} \frac{\partial f}{\partial \phi_{pf}} \right)$$

$$\left(\lambda = \frac{3\epsilon_{pf}\sigma}{\sqrt{8}}, \qquad \gamma_{pf} = \xi \epsilon_{pf}^2 \right)$$

As mentioned above, the first and second equations are the continuity and momentum equations for investigating the fluid phenomena. The effect of magnetic force can also be investigated by adding the magnetic force term to the RHS of the momentum equation. This will also be discussed in a later section.

The third equation is the phase-field equation to track the slug interface. In the phase-field equation, ϕ_{pf} is the phase-field variable for interface tracking. From this, as in the level-set method, the LHS gives the correct motion of the interface. In this case, the convective term $(u \cdot \nabla \phi_{pf})$ of the phase-field equation is in a non-conservative form. If the convective term is in a non-conservative form, it can induce some numerical errors, such as mass loss. However, it can yield good results for most situations and usually converges more easily. It will be verified that this convective term can give good results for slug movement. On the RHS, ϵ_{pf} is the controlling parameter related to the thickness of the interface, and γ_{pf} is the mobility related to the time scale of the interface diffusion. Additionally, ψ can be expressed by the phase-field variable (ϕ_{pf}), interface thickness controlling

parameter (ϵ_{pf}), mixing energy density (λ) and external free energy (f). The mixing energy density (λ) is related to the surface tension. Thus, it can be expressed by the surface tension and interface thickness controlling parameter, as discussed above. For stability of the system, the RHS of the phase-field equation strives to minimize the total free energy with a relaxation time controlled by the mobility. For the mobility (γ_{pf}), to retain a constant interface thickness, the mobility should be large enough. However, if it is too large, the convective terms can be overly damped. In COMSOL Multiphysics, the mobility is determined by a mobility turning parameter (ξ) that is a function of the interface thickness, as discussed above. Thus, the proper value of the mobility parameter should be used for the simulation. In this study, the default value of the mobility parameter ($\xi = 1$) is used to investigate the slug movement. This value can give good results for most cases [24], and it will be validated in a later section.

3.2. Conditions for simulation

The schematic of simulation for slug movement is represented in figure 3.1.
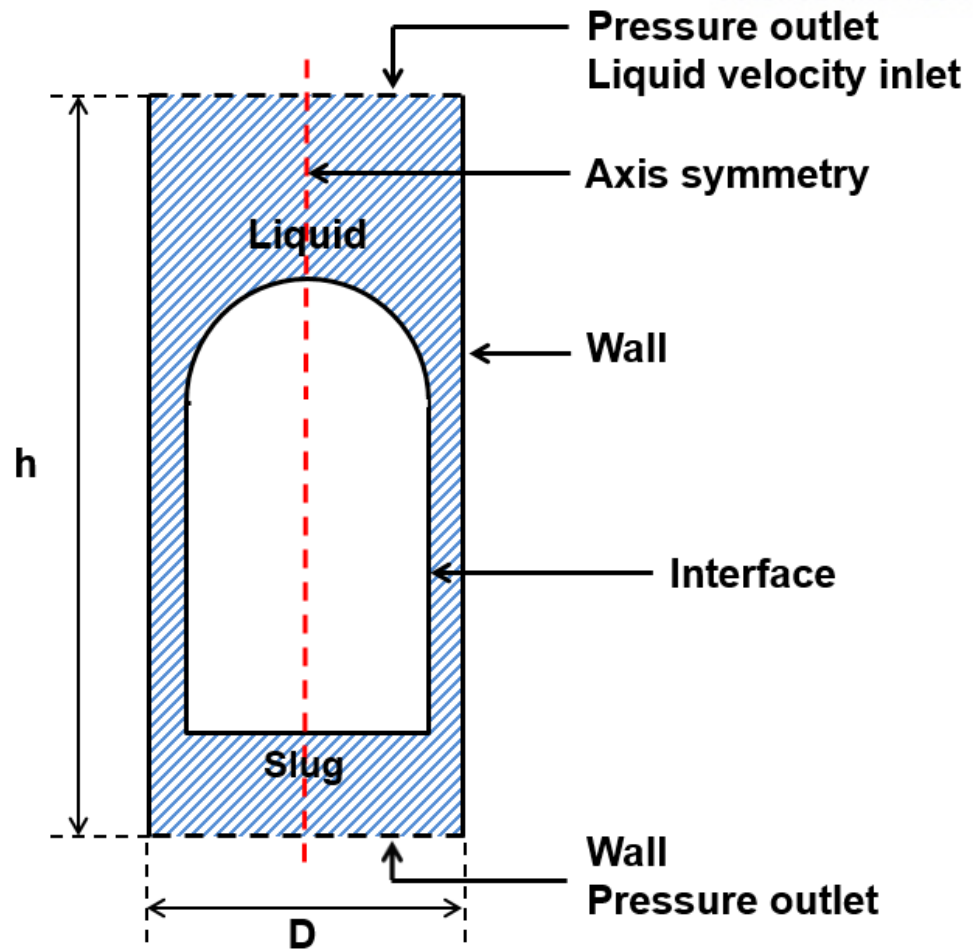
Figure 3.1. Schematic of slug simulation

In figure 3.1, the flow field is initially filled with any liquid, and the slug is placed in it. One of the side boundaries (walls) is treated as a no-slip boundary condition, and the other is an axis-symmetric boundary condition. When the slug moves in stagnant liquid, the top and bottom boundaries are treated as a pressure outlet and no-slip wall, respectively. The slug movement with liquid backflow is also investigated in this study because it can occur in real situations. Thus, the top boundary is treated as a liquid velocity inlet and the bottom is treated as a pressure outlet when the slug moves with liquid backflow. The width of the fluid domain is 10 mm, and height is 150 mm. In addition, the initial interface of gas and liquid is set as in figure 3.1. As in the bubble investigation, the steam is used as the slug, and EFH1 and EFH3 are used as the surrounding liquid.

Additionally, as in the bubble simulation, the computational domain is constructed with fixed triangular meshes uniformly over the entire domain to investigate the slug movement. The number of

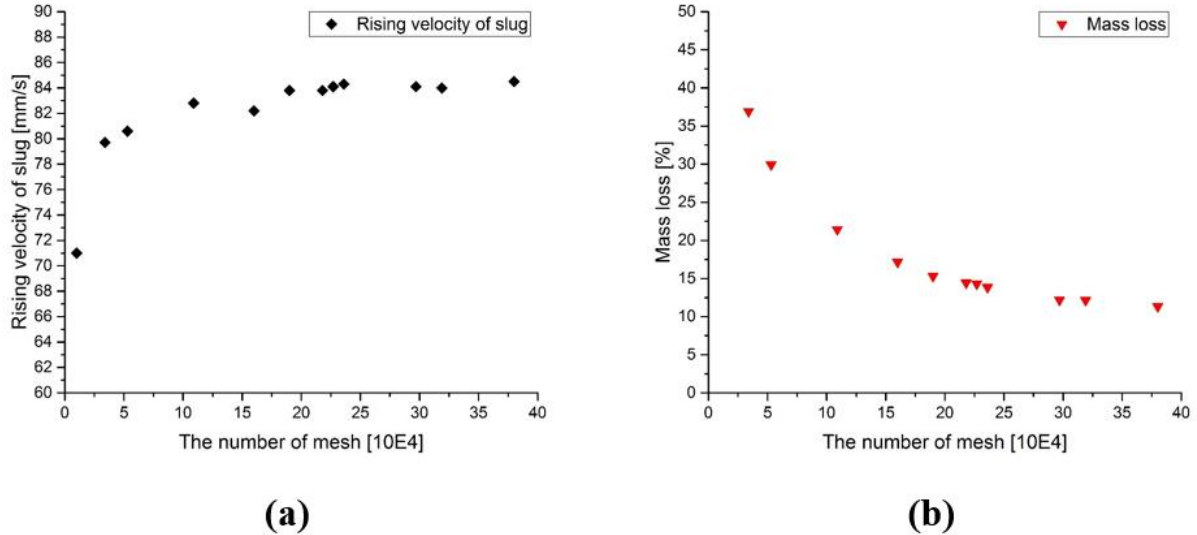elements can affect the simulation results, as shown in figure 3.2.

Figure 3.2. Mesh dependency test; (a) Rising velocity of slug, (b) Amount of mass loss

Figure 3.2 presents the slug rising velocity and the amount of gas dissolution (mass loss) based on the number of elements. Unlike with bubble simulation, in this case, a small amount of mass loss can be generated because the convective term is set as a non-conservative form for easy convergence of the calculation. In figure 3.2, it is observed that both parameters are changed when the number of elements is increased. However, they become nearly constant when the number of elements is larger than 300,000. Thus, the following studies are conducted with 300,000 elements in this study.

3.3. Validation of the solver

In this part, the solver that is used for investigating the slug movement is validated by comparing the numerical results with previous research studies and experimental data.

3.3.1. Comparison with previous research studies.

From the previous research [12], the characteristics of the slug can be explained by some of the

dimensionless numbers. First, the three dimensionless numbers related to the slug characteristics are introduced below.

Froude number

$$Fr = \frac{U}{\sqrt{gD}} \tag{3-5}$$

Eotvos number

$$Eo = \frac{(\rho_l - \rho_g)gD^2}{\sigma} \tag{3-6}$$

Morton number

$$Mo = \frac{g(\rho_l - \rho_g)\mu_l^4}{\rho_l^2 \sigma^3} \tag{3-7}$$

Like bubble dynamics, these three dimensionless numbers are related to the fluid properties (viscosity, density, and surface tension), gravity acceleration and rising velocity of the slug. Unlike bubbles, however, these dimensionless numbers include the diameter of the fluid domain instead of the bubble diameter because the diameter of the slug is determined by the domain size. In other words, the characteristics of the slug can be determined by these three dimensionless numbers.
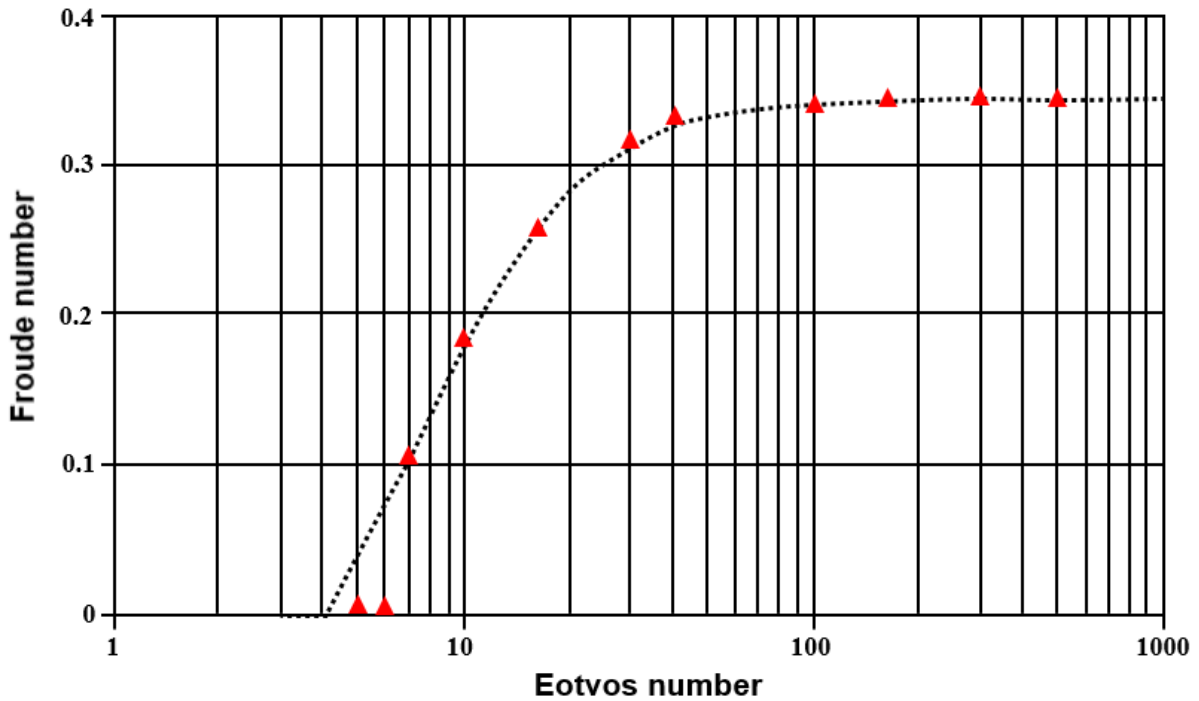
Figure 3.3. Slug rising velocity with different Eotvos number ($Mo<10^{-8}$), (·····) : White and Beardmore, (▲) : This study

Figure 3.3 represents the Froude number according to the Eotvos number variation when the Morton number is smaller than 10E-8. In figure 3.3, it is observed that the Froude number changes with the Eotvos number along the same course for a low-viscosity fluid (Mo<10E-8). This means that the viscosity of the liquid does not affect the slug velocity for low-viscosity fluids. Additionally, it is easily observed that the numerical results from this study agree well with previous research over a wide range of Eotvos numbers, with the exception of small Eotvos numbers (Eo < 7). For small Eotvos numbers, the slug cannot rise because the buoyancy force is smaller than the friction drag force. As the Eotvos number is increased gradually, the buoyancy force becomes larger, and finally the slug can rise at any Eotvos number. This can be called the critical Eotvos number. For the critical Eotvos number, many previous research studies have reported slightly different values. Thus, more research on this is necessary. However, the solver can provide good results regarding slug movement for low-viscosity liquids when the Eotvos number is not small.
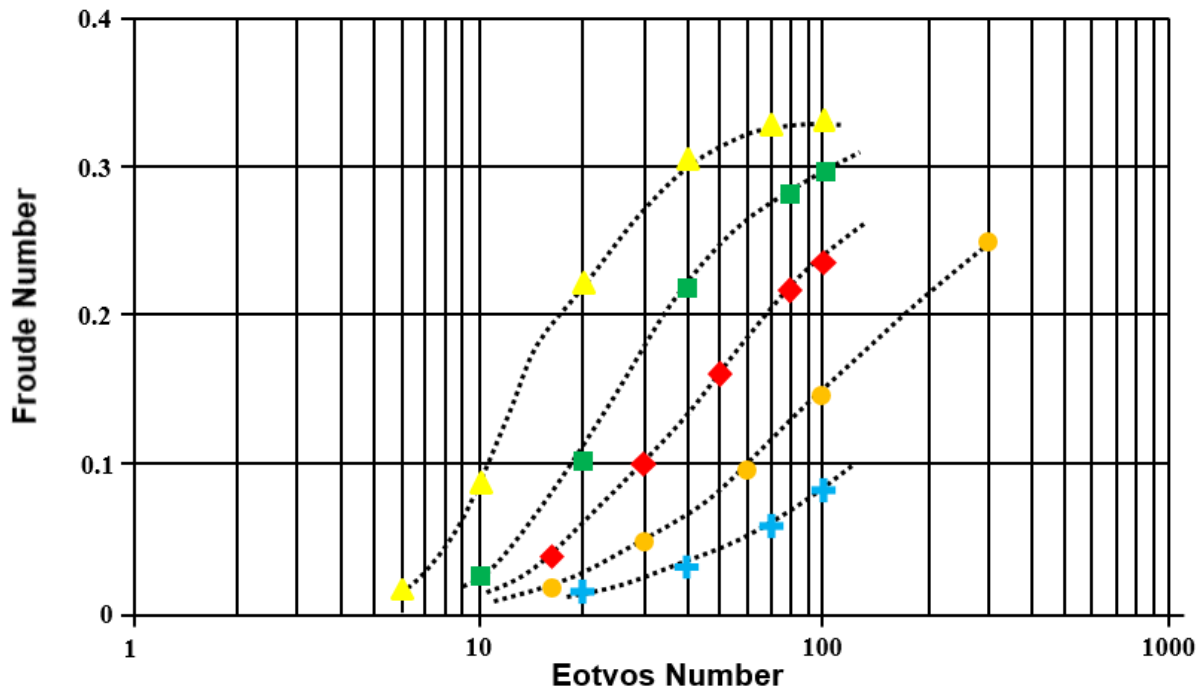
**Figure 3.4. Slug rising velocity with different Eotvos number (Various Morton number), (·····) :
Taha and Cui;**

**This study (▲) : $Mo = 4.7 \times 10^{-5}$, (■) : $Mo = 1.6 \times 10^{-2}$, (◆) : $Mo = 0.33$, (●) :
$Mo = 8.0$, (✚) : $Mo = 100$**

Figure 3.4 represents the Froude number according to the Eotvos number variation for various Morton numbers (higher than 10E-8). In figure 3.4, it is observed that the variation of the Froude number with the Eotvos number can be different if the Morton number is larger than 10E-8. This means that the viscosity is important to the slug velocity for high viscous liquids because the Morton number can be changed by the viscosity. It is also easily observed that the numerical results agree well with previous research for various Morton numbers. Thus, figure 3.4 shows us that the solver can also provide good results for high viscous liquids.

In this study, the slug movement in magnetic nanofluid is investigated, and the domain diameter is 10 mm. For the EHF1, the Eotvos number and Morton number are 40.9 and 4.3E-7, respectively. For the EFH3, the Eotvos number and Morton number are 48.0 and 5.9E-6. Thus, the results can be reliable because neither case is included in the uncertain region (below the critical Eotvos number). In

addition, all cases for validation are simulated with the default value of γ_{pf} and a non-conservative convective form. Thus, reliable results can be provided for slug movement.

3.3.2. Comparison with experimental data

In this study, the slug movement is also observed by experiment. The experiment for slug movement is introduced in this part, and the numerical solver is validated again by comparing the numerical results with the experimental data. Additionally, the shape of the slug is discussed in a simple manner.
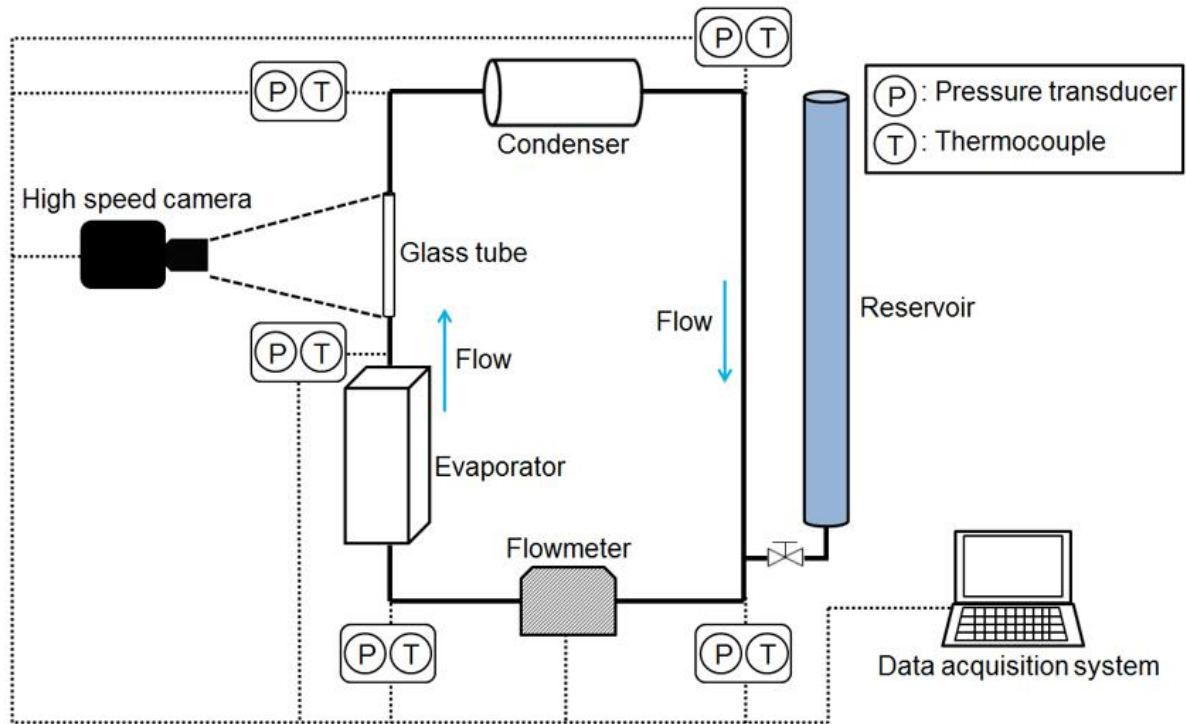
Figure 3.5. Schematic of experimental apparatus (Slug movement)

Figure 3.5 represents the schematic of the slug experiment. It consists of a loop thermosyphon and high-speed camera. The loop thermosyphon consists of an evaporator, condenser, reservoir, glass tube, stainless tube, flowmeter, 5 pressure transducers and 5 thermocouples. The glass tube is placed at the exit of the evaporator to observe the slug movement. The diameter of the glass tube is 10 mm, and the

height is 150 mm. It is the same size as in the simulation. The test fluid is DI-water and HFE7300.

The loop is initially filled with fluid, and heat is transferred to the fluid by the evaporator (100 W). As time passes, the vapor is generated by boiling, and it is moved upward along the glass tube. Then, the residual heat is removed by the condenser to achieve a stable condition. From the measuring equipment, such as the thermocouples, pressure transducers and flowmeter, the steady state of the system can be found. Then, the slug movement is captured through the glass tube by using the high-speed camera. From this experiment, the slug of DI-water and HFE 7300 is observed, and these conditions are numerically simulated to compare the results.
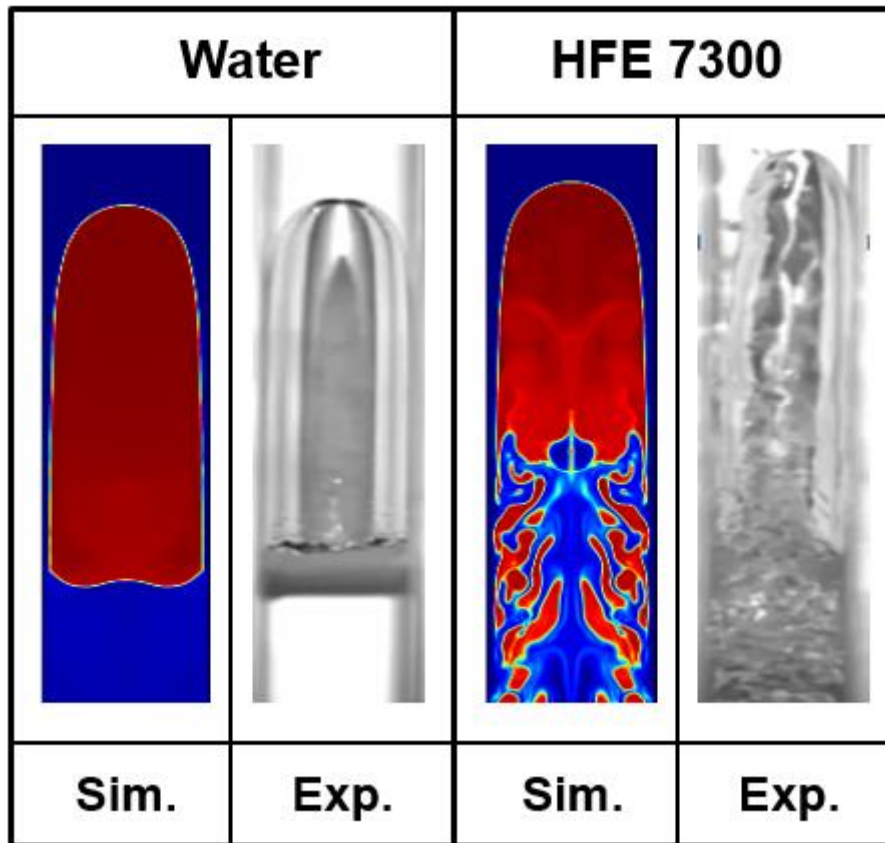

Figure 3.6. Comparison of slug shape; Simulation vs Experiment

Figure 3.6 shows the shape of the slug in each fluid for the experiment and simulation. In this figure, it is observed that the surface of the slug in HFE7300 is rough and that the small bubbles are

generated at the rear of the slug. However, the surface of the slug in the DI-water is relatively smooth, and the small bubbles are not observed in this case. This can be explained by surface tension. The surface tensions of the DI-water and HFE 7300 are 0.05891 [N/m] and 0.00885 [N/m], respectively. The surface tension of the DI-water is much higher than that of HFE 7300. Consequently, the slug in the DI-water has much higher interfacial force than HFE 7300. Thus, the surface of the slug can be stable, and the small bubbles cannot be separated from the slug body in DI-water. However, the slug in HFE7300 has relatively low interfacial force because of the low surface tension. Thus, the surface of the slug becomes unstable, and the small bubbles can be separated from the slug body. In addition, in figure 3.6, it is easily observed that the simulation results correspond well with the experimental results. Thus, the solver used in this study can provide reliable results for the slug shape.

3.4. Results and discussion

3.4.1. Effect of solid particles and slug length

In this part, the effect of solid particles is investigated for slug movement and shape. As in the bubble investigation, the effect of solid particles can be observed by comparing the results in EFH1 and EHF3 because each magnetic fluid contains different amounts of solid particles.
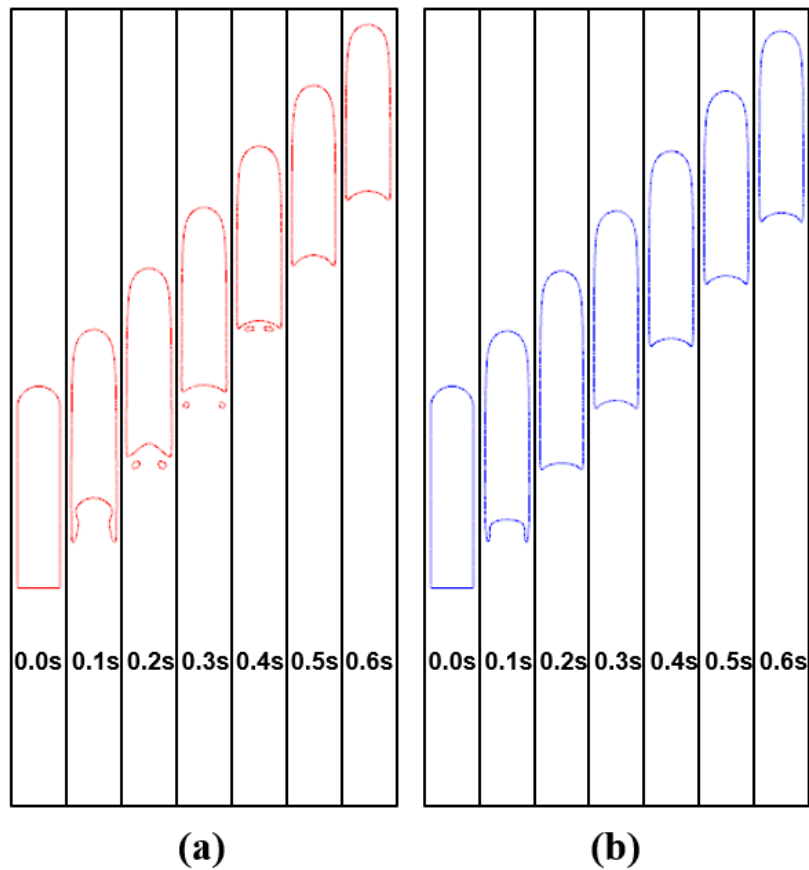
Figure 3.7. Single slug movement in each magnetic fluid; (a) EFH1, (b) EFH3

Figure 3.7 represents the slug movement in each magnetic fluid, and slug length is 38 mm in this case. In figure 3.7, it is observed that the slug in EFH1 rises slightly faster than that in EHF3. As in bubble movement, this can be explained by the viscosity of the fluid. The viscosity of EFH3 is higher than that of EHF1 because of the additional solid particles. Thus, higher viscous friction drag can act on the slug in EFH3 than in EHF1. Because of this, the slug in EFH1 rises faster than that in EFH3. This effect is observed regardless of the slug length, as shown in figure 3.8.
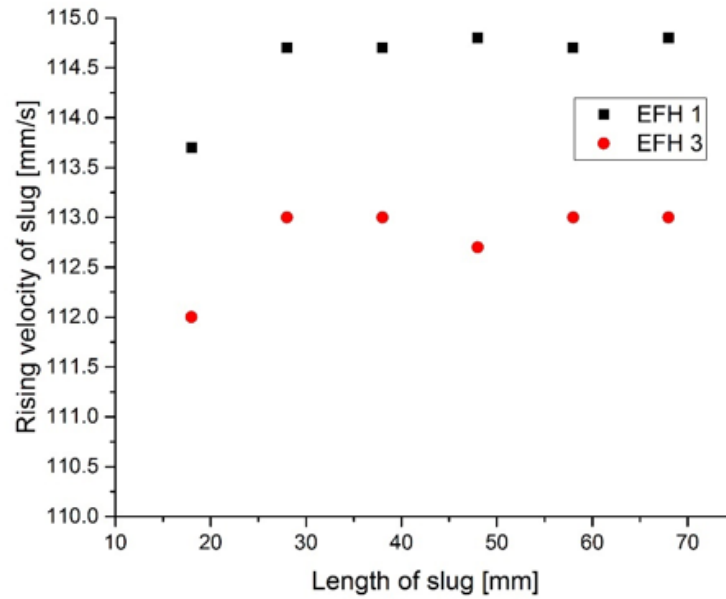
Figure 3.8. Slug rising velocity with different slug length

Figure 3.8 represents the slug's rising velocity with different slug lengths for EFH1 and EFH3. The slug is faster in EFH1 than in EFH3, regardless of slug length. Additionally, it is observed that the slug's rising velocity is nearly the same regardless of its length, except for only one case (L=18 mm). This is observed in both magnetic fluids. When the slug moves in liquid, the surrounding liquid is also moved by the slug movement as a thin film near the slug body. Thus, this effect can be explained by observing the velocity distribution of the liquid film.
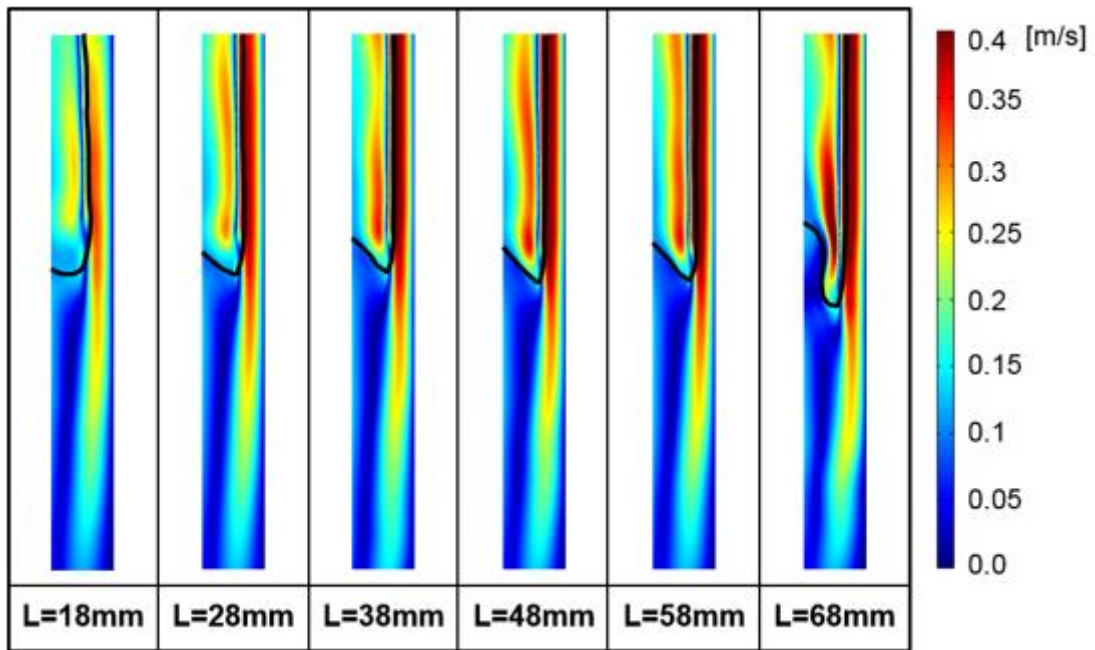
(a)
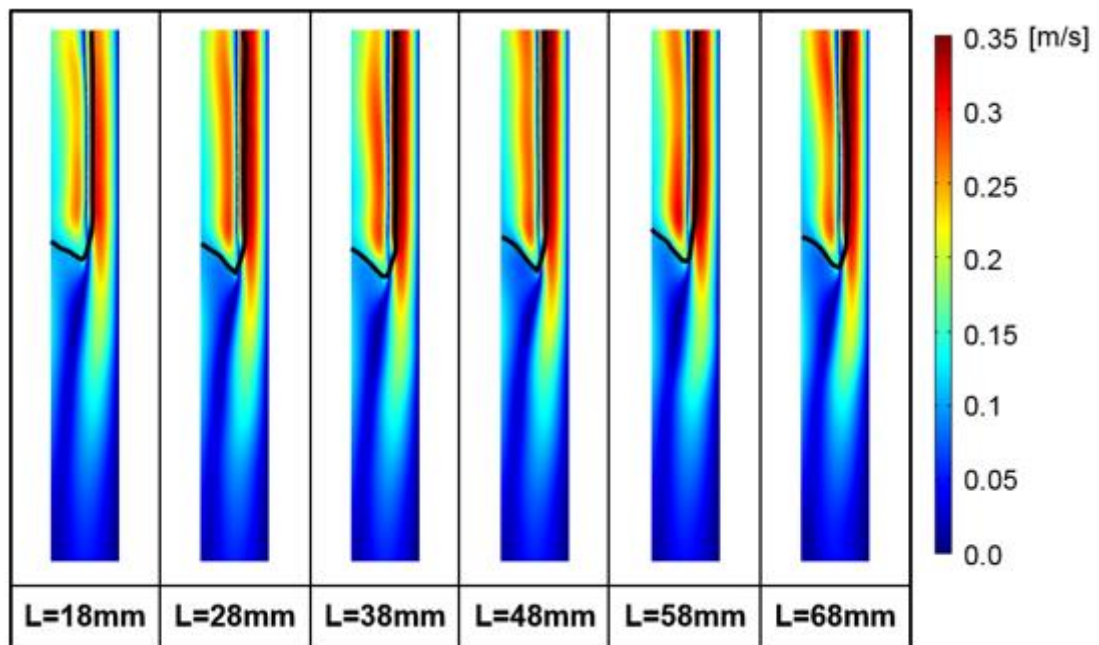
(b)

Figure 3.9. Velocity distribution of liquid film, (a) EFH 1, (b) EFH 3

Figure 3.9 represents the velocity field of the liquid film between the slug surface and wall for each case. In figure 3.9, it is observed that the velocity distribution of the liquid film is nearly the same in each case except for the L=18 mm case for each magnetic fluid. When the slug rises in the liquid, the liquid ahead of the slug moves downward between the slug surface and the wall as a thin film. This liquid film is accelerated gradually along the slug body, and its velocity finally reaches a terminal velocity. Then, the velocity of the liquid film is barely changed along the slug body (fully developed). This means that the drag force, such as the viscosity force, is balanced with the acceleration force after the liquid film velocity reaches its terminal value. Because of this, the rising velocity of the slug is not changed if the slug is long enough.
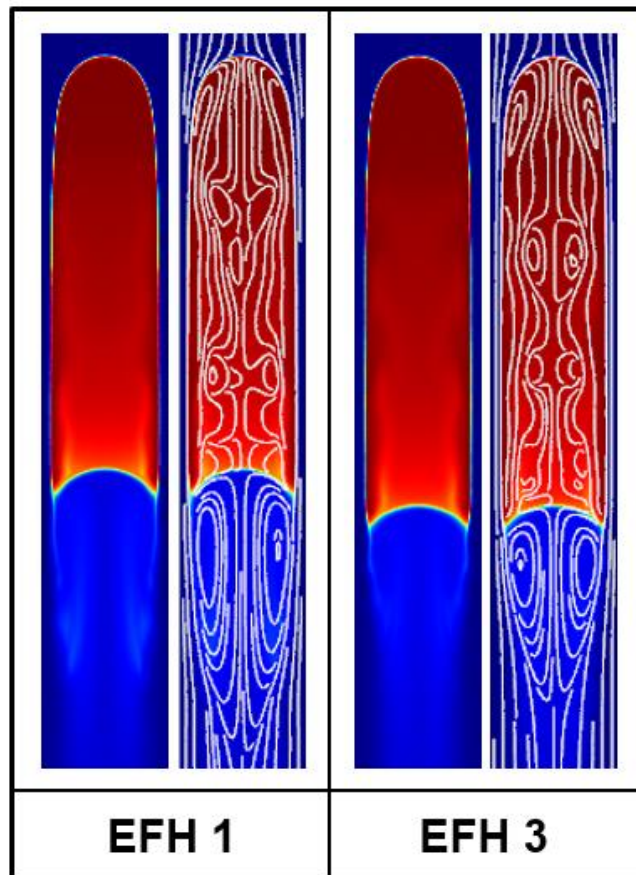

Figure 3.10. The shape and wake of slug in EFH1 and EFH3

Figure 3.10 represents the slug shape and the streamline distribution for each magnetic fluid. First, it

38

is observed that the slug in the EFH3 is slightly more stretched than in EFH1 because a higher viscous drag is acting on the slug in EFH3. In the streamline distribution, it is observed that the recirculation flow is generated at the rear of the slug in each magnetic fluid. However, the recirculation region is larger in EHF1 than EFH3. In Compos and Carvalho's research [13], they reported that the wake characteristics at the rear of the slug can be determined by the gravity acceleration, fluid domain diameter and kinematic viscosity when the slug moves in stagnant liquid. Regarding this, they suggested a dimensionless number.

$$N_f = \frac{(gD^3)^{1/2}}{\nu} \tag{3-8}$$

As we can see, this dimensionless number consists of the gravity acceleration, fluid domain diameter and kinematic viscosity. From this dimensionless number, they first identified the wake pattern at the rear of the slug. They reported that the closed recirculation wake is observed for $N_f < 1000$ and that the opened wake with recirculation flow, such as vortex shedding, is observed for $N_f > 1000$. They also said that the length of the closed recirculation wake is increasing with the increase of N_f. In the present study, for each magnetic fluid, the N_f values of EFH1 and EHF3 are 631.6 and 370.6, respectively. Thus, the closed recirculation wake is generated in both magnetic fluids, and the length of the recirculation wake is longer in EFH1 than in EHF3.

The interaction of two slugs is also investigated in each magnetic fluid to observe the effect of solid particles on slug interaction. In this study, the front slug remains at rest by liquid backflow because the slug movement should be observed over a long time to investigate the interaction of slugs. This can give good results for the investigation of the interaction pattern.
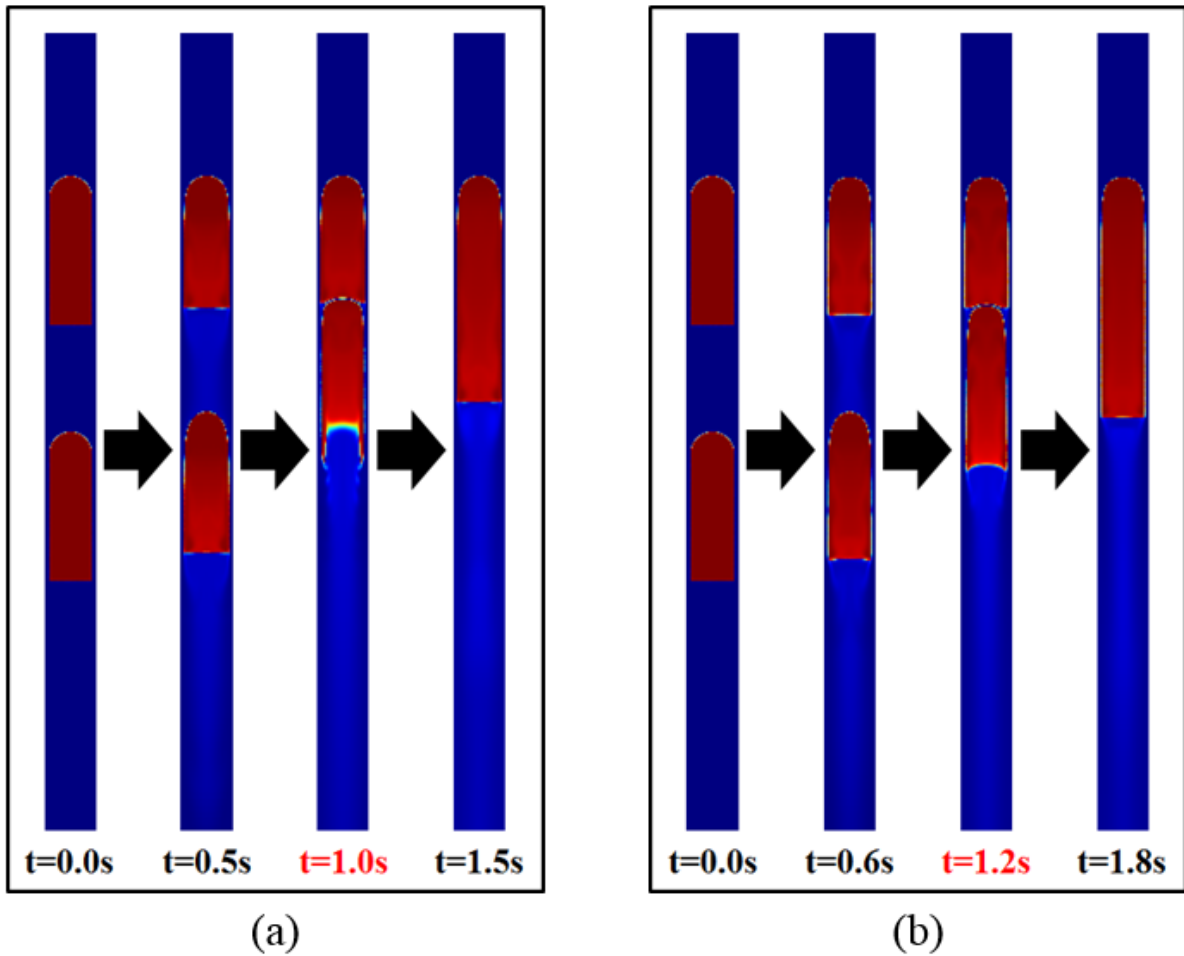
Figure 3.11. Interaction of two slugs in each magnetic fluid, (a) EFH 1, (b) EFH 3

Figure 3.11 represents the interaction of two slugs in each magnetic nanofluid. In both cases, the rear slug is gradually accelerated because the relatively small drag force is acted on it by the front slug. Thus, the rear slug moves to the front slug, and finally, the two slugs are merged as a long slug. Although this situation is observed in both cases, the slugs in EHF3 need more time for the merging than in EHF1 because the slug in EFH3 is slower than in EFH1 due to the viscosity difference. Thus, the amount of solid particles can also affect the interaction of slugs.

In this part, the single slug's movement and the interaction of the two slugs are investigated in each magnetic fluid. The slug length does not affect the slug velocity if it is long enough. Additionally, the amount of solid particles can affect the slug velocity, shape, wake and interaction. These results may

be useful for generating electrical energy by using the magnetic nanofluid and slug movement.

3.4.2. Effect of liquid backflow

When the slug rises in liquid, it can push any amount of liquid upward because its diameter is nearly the same as that of the fluid domain. Consequently, this liquid can flow downward and affect the slug movement. Thus, the slug movement in downward flowing liquid is investigated in this section.

Figure 3.12. Movement and wake of slug with different liquid backflow velocity in EFH 1;

(a) U=0.0m/s, (b) U=0.025m/s, (c) U=0.05m/s, (d) U=0.075m/s

Figure 3.12 shows the slug movement and the streamline distribution according to the velocity of the liquid backflow in EFH 1. In this figure, it is observed that the slug's rising velocity is decreasing when the velocity of the liquid flow is increasing. Additionally, the length of the recirculation flow is decreased when the velocity of the liquid backflow is increasing. These phenomena are also observed in EFH 3.
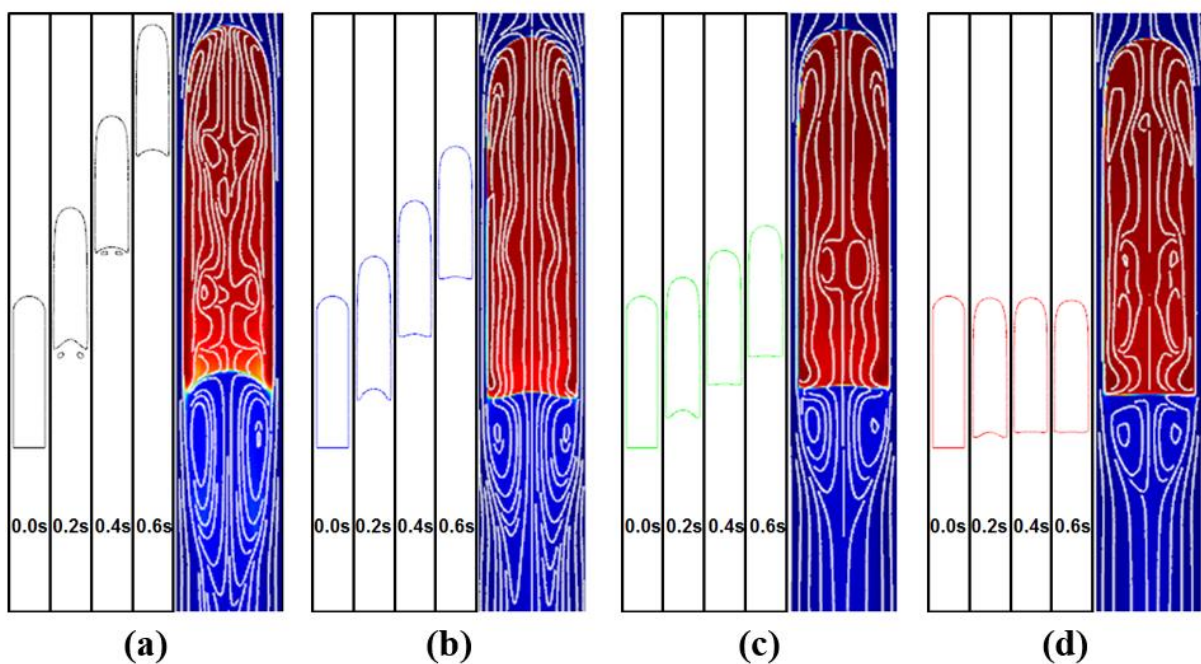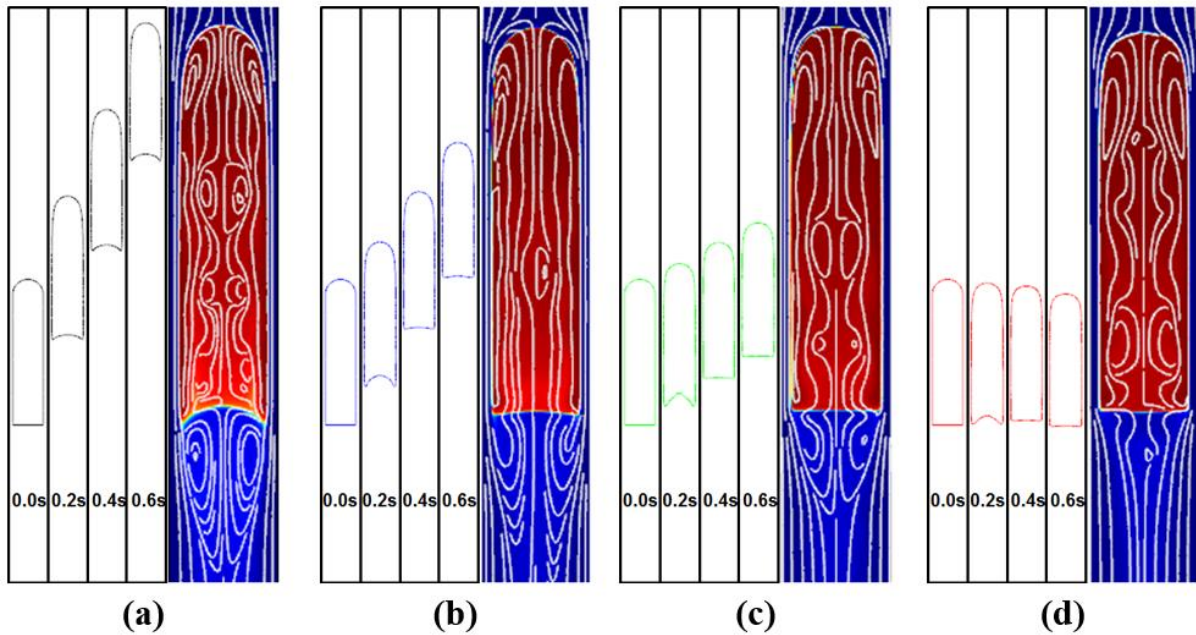
Figure 3.13. Movement and wake of slug with different liquid backflow velocity in EFH 3;

(a) U=0.0m/s, (b) U=0.025m/s, (c) U=0.05m/s, (d) U=0.075m/s

Figure 3.13 represents the slug movement and the streamline according to the velocity of the liquid backflow in EFH 3. In this figure, it is also observed that the slug's rising velocity is decreased when the velocity of the liquid backflow is increasing. The length of the recirculation flow is decreased when the velocity of the liquid backflow is increasing, as in EFH1. In this case, the recirculation flow disappears when the liquid velocity is 0.075 m/s. This means that the rising motion of the slug is more important than the liquid flow for generating the recirculation flow.

In this part, the slug movement in flowing liquid is investigated. The rising motion of the slug is an important factor for the recirculation flow at the rear of the slug. Additionally, a larger recirculation flow can be generated in EFH1 than in EFH3 regardless of the liquid flow.

3.4.3. Effective slug movement for energy generation

In this part, the effective slug movement is predicted to generate electrical energy more effectively. As

in the bubble investigation, the movement patterns of two slugs are first investigated.

| t=0.0s t=0.3s t=0.6s t=0.9s | t=0.0s t=0.5s t=1.0s t=1.5s | t=0.0s t=0.8s t=1.6s t=2.4s |
| (a) | (b) | (c) |
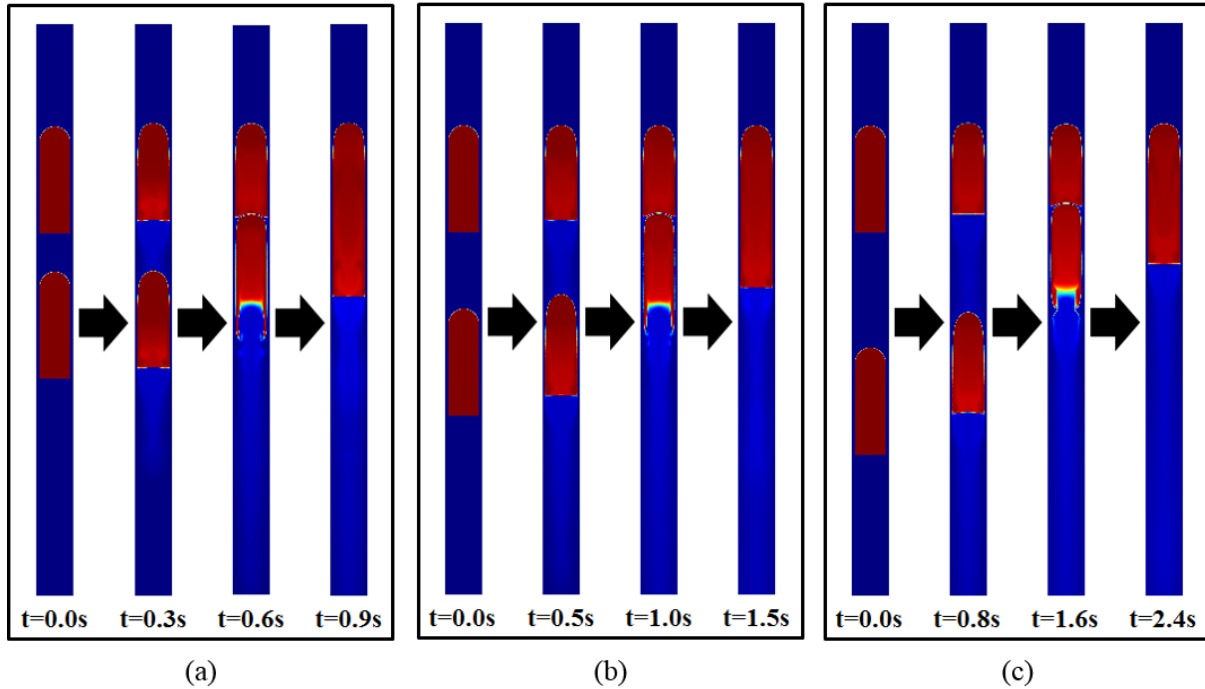
Figure 3.14. Interaction of two slugs, (a) s=10mm, (b) s=20mm, (c) s=30mm

Figure 3.14 represents the interaction of two slugs according to the initial distance between each slug. In all cases, the rear slug is gradually accelerated and moves to the front slug, and the two slugs are finally merged with each other because the relatively small drag force is acting on the rear slug, as mentioned above. Only the time of merging is different for each case. The interaction pattern of two slugs is not varied unlike with bubble interaction because the slug can move only along the pipe. Thus, effective slug movement can be predicted by observing the velocity field and streamline of each case.

Figure 3.15. Velocity field and streamline of each case, (a) s=10mm, (b) s=20mm, (c) s=30mm

Figure 3.15 shows the velocity field and streamline distribution for each case. In the velocity distribution, it is observed that the surrounding magnetic fluid has a relatively large velocity magnitude when two slugs are merged with each other for all cases. This means that the magnetic field can be disturbed more actively by the magnetic fluid when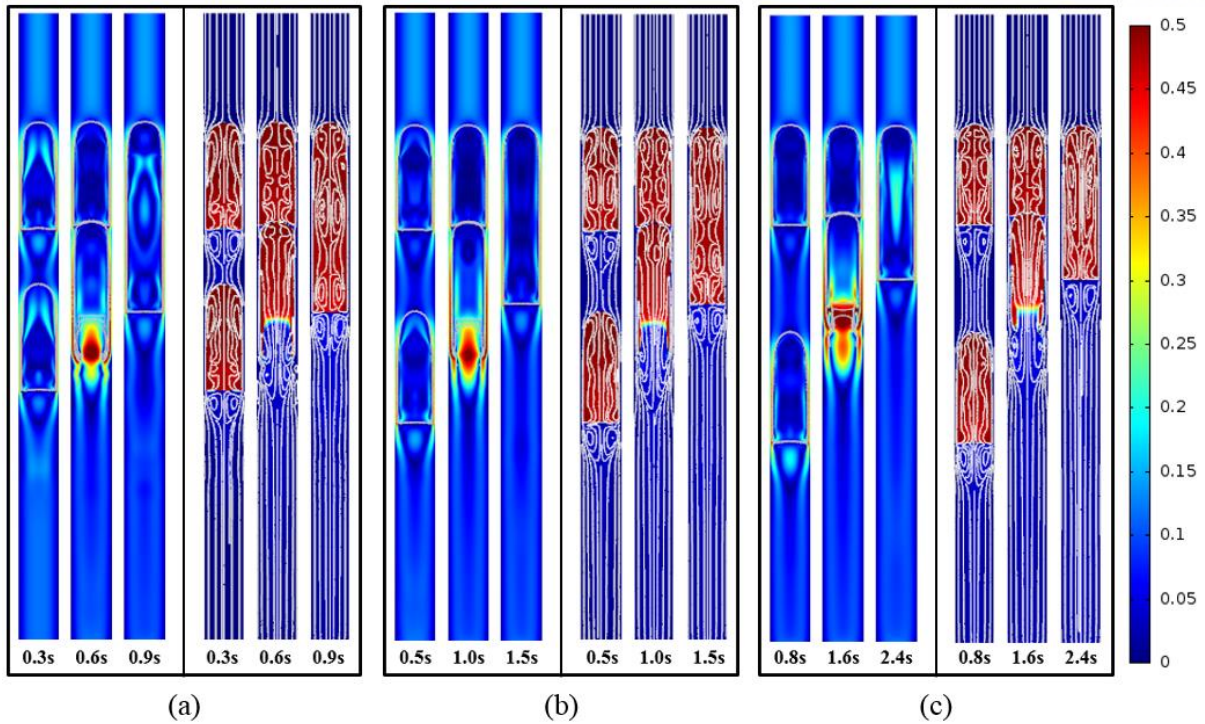 two slugs are merged. Thus, the merging of slugs may be effective for energy generation. In the streamline distribution, it is observed that the size of the recirculation flow is nearly the same for each short slug and the long slug. However, the recirculation region grows larger, to nearly twice the value, when the two slugs are merged with each other. Thus, if the merging occurs or small slugs move, it may be effective for energy generation because the magnetic field can be actively disturbed.

As mentioned above, however, it is just an approximate analysis. The movement of magnetic fluid should be evaluated quantitatively for reliable prediction. Thus, the average velocity of only the magnetic fluid is calculated as in the bubble investigation. Unlike the bubble simulation, the liquid is flowing downward in this case because it should be observed over a long period of time. However, it is applied equally to all cases. Thus, the effective condition can be found regardless of liquid backflow.

44
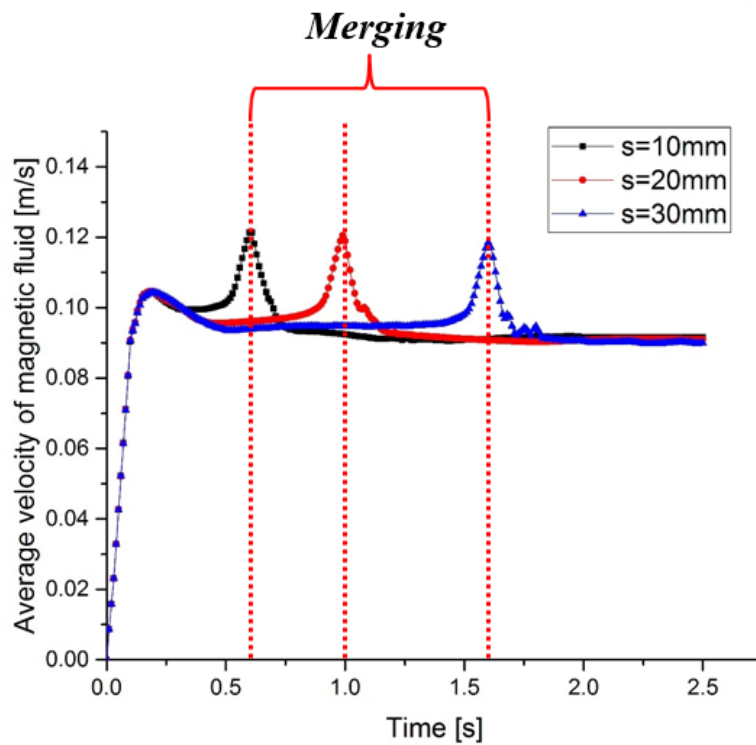
Figure 3.16. Average velocity of surrounding liquid for each case

Figure 3.16 represents the average velocity of the magnetic fluid for each case. Initially, the average velocity of the magnetic fluid is 0 for all cases. As time passes, the velocity of the magnetic fluid is increasing gradually because of the slug movement and liquid flow. For all cases, a temporarily much larger velocity is observed when the two slugs are merged. This means that the magnetic fluid is moved more actively by the merging of slugs. Thus, the merging of slugs can be effective for energy generation. In addition, it is observed that the average velocity of the magnetic fluid is slightly larger before merging than after. This means that the motion of small slugs can be slightly more effective than that of one large slug.

In this part, the effective slug movement is investigated for energy generation. Unlike with bubble movement, the merging of slugs can be effective for energy generation. Additionally, the small slugs can be more effective than one large slug.

4. Investigation of the magnetic force effect

In the energy generation idea, the magnetic field should be applied to the system to generate electrical energy by Faraday's law. Consequently, the magnetic force can act on the flow field. Thus, the effect of the magnetic force is investigated for bubble and slug movement in this section.

4.1. Theory for investigation

When the magnetic field is applied to any material, this material is magnetized by the magnetic field. At this time, the magnetization value of the material can be determined by the strength of the magnetic field and its magnetic permeability. In other words, when any value of magnetic field is applied to the system, the magnetization value of each material is determined by its magnetic permeability. For convenience, the magnetic permeability of any material can be expressed by the permeability of a vacuum as shown below.

$$\eta_r = \frac{\eta}{\eta_0} = \chi + 1 \tag{4-1}$$

In the above equation, η_r is the relative permeability of any material, η is the magnetic permeability of any material, and η_0 is the magnetic permeability of a vacuum, which is $4\pi \times 10^{-7}$ [H/m]. As we can see, the relative permeability of a material (η_r) can be expressed as a ratio of η and η_0. Additionally, χ is the magnetic susceptibility, which can be expressed as $\chi = \eta_r - 1$. Thus, it also represents the magnetization value of a material. The magnetization value of any material can be determined by the above variables when the magnetic field is applied to the system. In addition, the magnetic force can act on any material when it is magnetized by an external magnetic field. Thus, the magnetic force effect should be considered if a magnetic field is applied to any system. In this study, gas bubble and slug movement in a magnetic fluid is investigated. Thus, an investigation regarding a magnetic force in the flow field is necessary. When the magnetic field is applied to a flow field without an electric current, the magnetic force acting on the unit volume of fluid can be calculated by the below equation [20].

$$F_m = \frac{1}{2}\eta_0 \chi \nabla H^2 \tag{4-2}$$

46

In the above equation, H represents the magnetic field strength at a fluid element. From the above equation, the total magnetic force acting on a bubble or slug can be calculated to predict the direction of the magnetic force.

$$F_{m,t} = \frac{1}{2}\eta_0(\chi_g - \chi_l)\int \nabla H^2 dVol \qquad (4\text{-}3)$$

In the above equation, χ_g and χ_l are the magnetic susceptibility of gas and the surrounding liquid, respectively. If $(\chi_g - \chi_l)$ is a (+) value, the magnetic force is acting on the maximum magnetic field. However, if $(\chi_g - \chi_l)$ is a (-) value, the direction of the magnetic force is opposite. In other words, if $(\chi_g - \chi_l)$ is a (+) value, the bubble and slug can be driven from a lower magnetic field location to a higher location. But if $(\chi_g - \chi_l)$ is a (-) value, the bubble and slug can be driven in the opposite direction. The direction of the magnetic force can be predicted as explained above. Finally, the momentum equation should be recast to investigate the fluid phenomena with the magnetic force by adding the above equation (4-2) as an external force, as shown below.

Momentum equation with magnetic force

$$\rho\frac{\partial u}{\partial t} + \rho(u \cdot \nabla)u = \nabla \cdot [-pI + \mu(\nabla u + (\nabla u)^T)] + \rho g + \frac{1}{2}\eta_0\chi\nabla H^2 \qquad (4\text{-}4)$$

Finally, the bubble and slug movement with the magnetic force can be investigated by solving the above equation.

4.2. Conditions for simulation

The schematic of simulation for investigating the magnetic force effect is represented in figure 4.1.
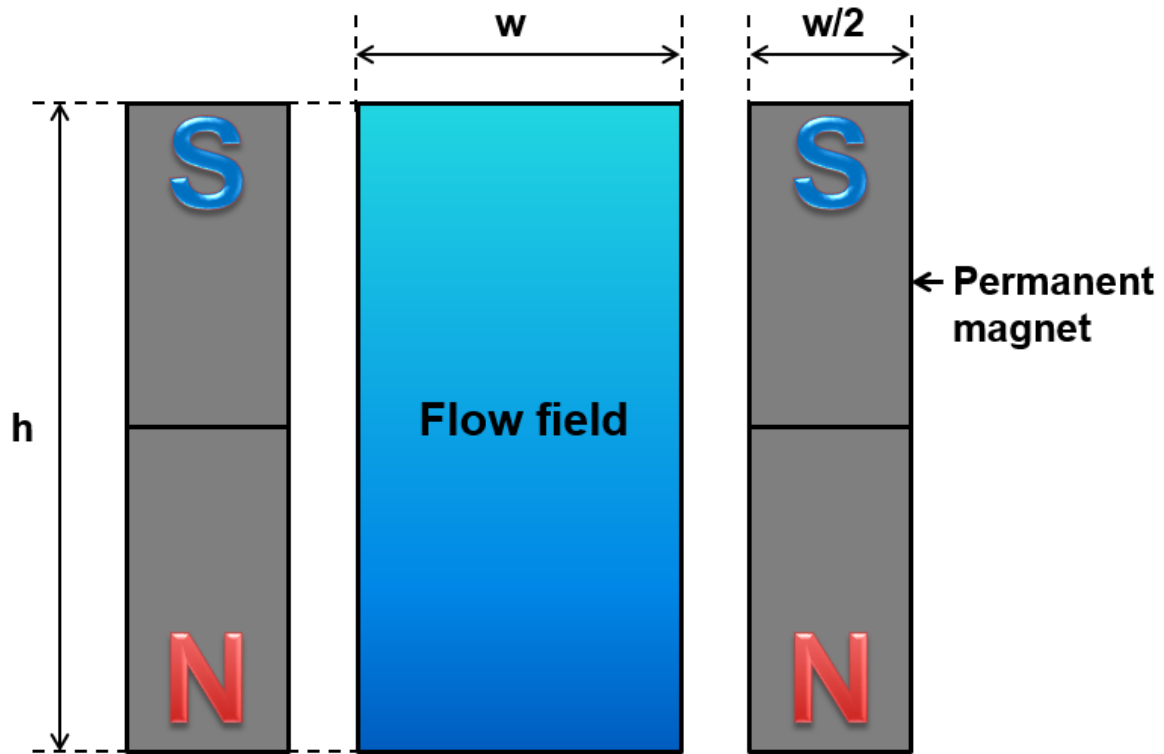

Figure 4.1. Geometric configuration of permanent magnet

In figure 4.1, two permanent magnets are placed at both sides of the flow field. The height of each magnet is the same as the fluid domain, and the width is half of the fluid domain. Additionally, the strength of each permanent magnet is 1.0 [T], and this value is general. The relative magnetic permeability of steam is -4.25×10^{-3}. Regarding the magnetic fluids, the relative magnetic permeability of EFH1 and EFH3 are 2.6 and 3.4, respectively. As we can see, the magnetic permeability of EFH3 is higher than that of EHF1 because the EFH3 contains a greater amount of magnetic particles. This means that a stronger magnetic force can be generated for EHF3 than EFH1. Thus, the EFH3 is only considered to investigate the effect of a magnetic force in this section. Under these conditions, the effect of a magnetic force is investigated for bubble and slug movement.

4.3. Results and discussion

4.3.1. Magnetic field distribution and direction of the magnetic force
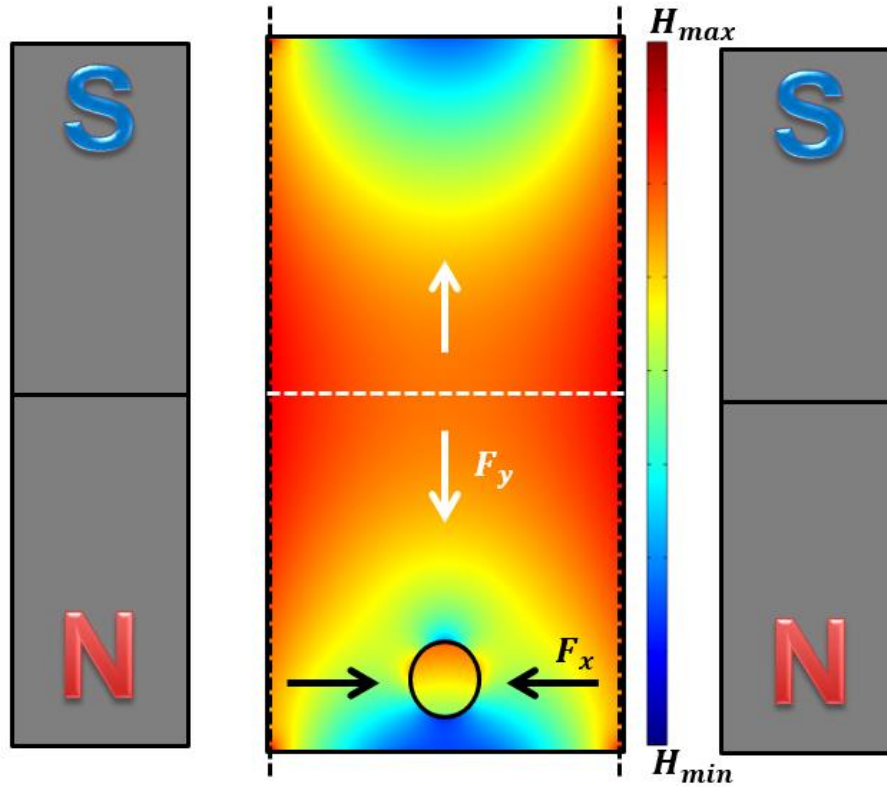
Figure 4.2. Magnetic field distribution and magnetic force direction

Figure 4.2 shows the magnetic field distribution and the direction of the magnetic force when the permanent magnets are placed at both sides of the flow field as shown in the figure. As we can see, in this case, the maximum magnetic field for the y-direction appears at the center of the flow field, and it appears at both sides of the flow field for the x-direction. Additionally, the value of $(\chi_g - \chi_l)$ is (-) for this case. Thus, as mentioned above, the magnetic force may act on the bubble and slug for each direction, as shown in figure 4.2.

4.3.2. Motion of a single bubble driven only by the magnetic force

Before applying the magnetic force in a real situation, the motion of a bubble driven only by the magnetic force is observed to ensure that the magnetic force model is applied correctly.
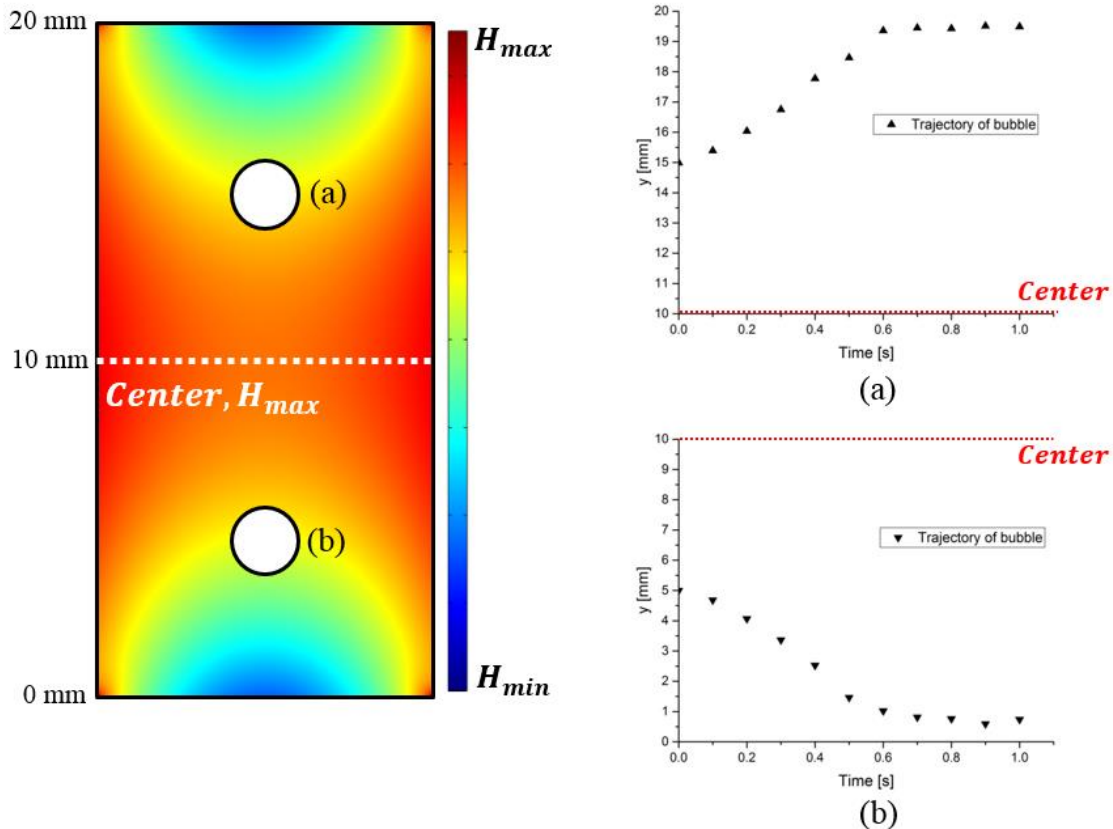
Figure 4.3. Trajectory of single bubble driven by only magnetic force

Figure 4.3 represents the initial position of the bubble and the trajectory of the bubble driven by the magnetic force for each case. In this case, the gravitational force is removed, and the value of the magnetic force is increased to 100 times the real value to clearly observe the effect of the magnetic force. The bubbles are initially placed at the upper and lower location rather than the center of the fluid domain as in figure 4.3. In figure 4.3, it is observed that each bubble moves in the opposite direction of the maximum magnetic field, as we predicted above, and each bubble is finally stopped by the wall. In other words, the bubble can be driven by the magnetic force, and it moves in the

opposite direction of the maximum magnetic field. Thus, it is confirmed that the magnetic force model is applied correctly in this simulation.

4.3.3. Effect of magnetic force for bubble and slug movement

In the previous section, it was confirmed that the magnetic force model is applied correctly in the present work. Thus, in this section, the magnetic force is applied to a real situation to investigate the effect of the magnetic force.

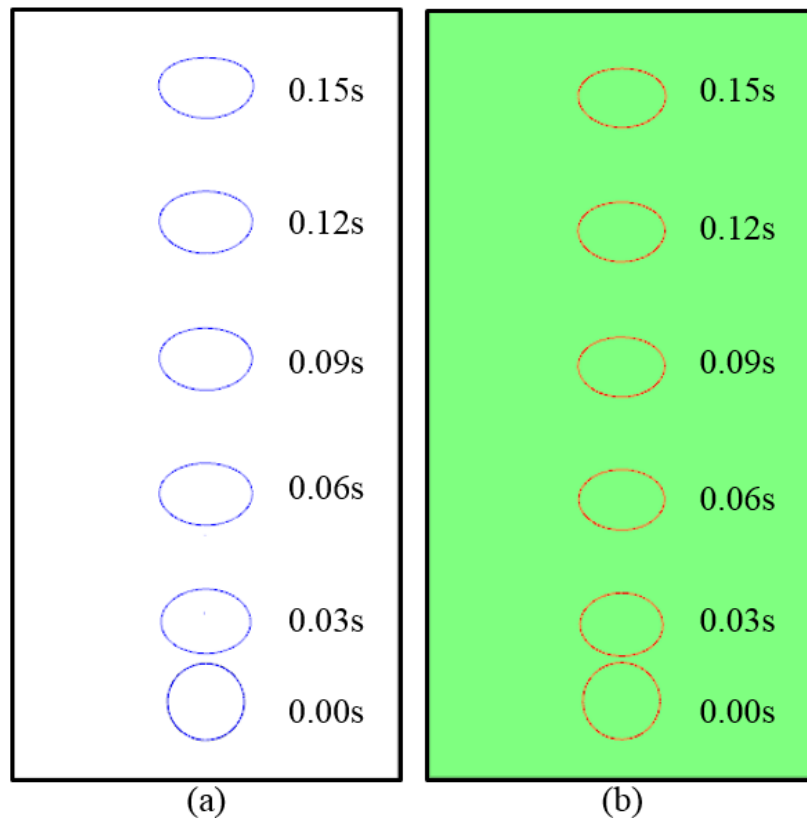**Figure 4.4. Single bubble movement in EFH 3, (a) w/o magnetic force, (b) w/ magnetic force**

First, figure 4.4 represents the motion of a single bubble with and without magnetic force. In this figure, the shape and rising velocity of each bubble are nearly the same. The reason for this result is that the value of the magnetic force is just nearly 1% of the gravitational force. Consequently, the

effect of the magnetic force cannot be observed in this case. Thus, the vertical magnetic force can be ignored when gravity is applied to the system.
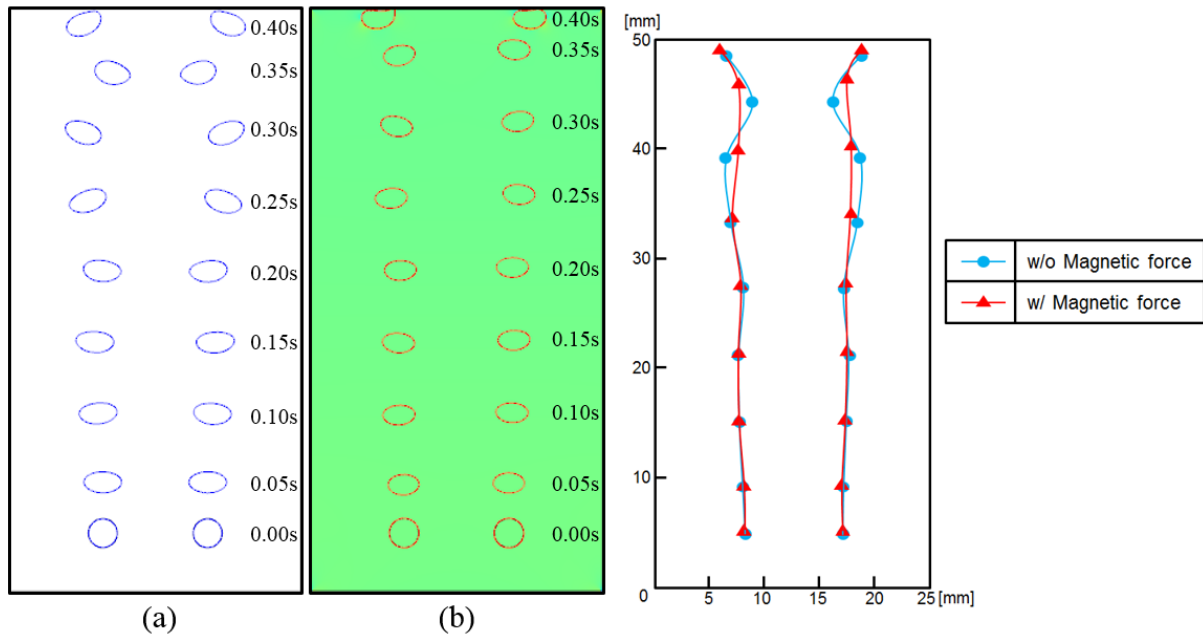

Figure 4.5. Interaction of two bubbles in EFH 3, (a) w/o magnetic force, (b) w/ magnetic force

Figure 4.5 shows the interaction of two bubbles with and without magnetic force. In this figure, the bubbles move upward in a straighter manner when the magnetic field is applied to the fluid domain because the horizontal magnetic force acts on the bubble and inhibits the bubble fluctuation. This means that the magnetic force can affect the bubble movement in the horizontal direction, unlike the case of the vertical direction. When the gas bubble moves in liquid, the buoyancy force in the vertical direction is dominant, and the hydrodynamic force in just the horizontal direction can be generated by the reaction of bubble movement and any obstacles, such as other bubbles or the wall. Thus, the hydrodynamic force can be much smaller for the horizontal direction than the vertical direction if the bubble is small enough and its velocity is not too large. Because of this, the magnetic force can affect the bubble movement in the horizontal direction, as in figure 4.5. However, the effect of the magnetic force in the horizontal direction is also very small because the difference of amplitude is just nearly 0.5 mm. Additionally, it cannot change the pattern of bubble movement. Thus, the effect of the horizontal magnetic force can also be ignored when gravity is applied to the system.

The effect of the magnetic force for slug movement is also investigated. From the above investigation, it is predicted that the magnetic force also cannot affect the slug movement.
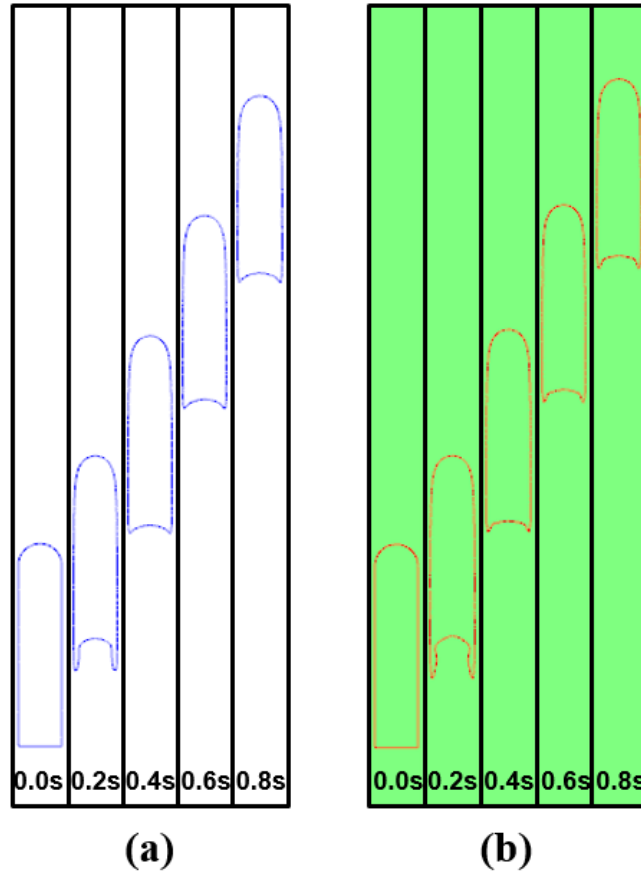

Figure 4.6. Single slug movement in EFH 3, (a) w/o magnetic force, (b) w/ magnetic force

Figure 4.6 represents the motion of a single slug with and without magnetic force. As we predicted, we do not observe much difference in each case because the hydrodynamic force is much higher than the magnetic force. Thus, the magnetic force also cannot affect the slug movement.
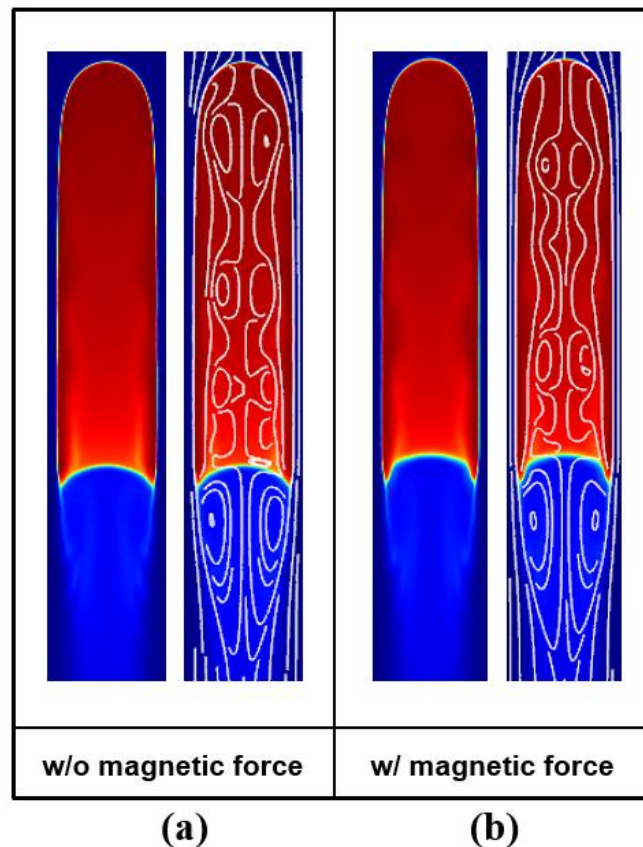
Figure 4.7. The shape and wake of slug in EFH 3, (a) w/o magnetic force, (b) w/ magnetic force

Figure 4.7 represents the slug shape and streamline for each case. In this figure, it is observed that the shape and wake of the slug is nearly the same for each case. Thus, the magnetic force also cannot affect the slug shape and wake.

In this part, the effect of the magnetic force is investigated for bubble and slug movement. The magnetic force does not affect the bubble and slug movement when gravity is applied to the system. In the horizontal direction, however, the magnetic force can slightly affect the bubble movement. It can also be ignored, however, because its effect is quite insignificant. Thus, the important factor for using magnetic fluid disturbance to generate electrical energy is not the magnetic force but the hydrodynamic force. Additionally, the effective motion of bubbles and slugs as investigated in the previous section is reliable even though it was investigated without magnetic force.

5. Conclusions

In this study, the idea is suggested to generate electrical energy by using magnetic nanofluid and gas bubble movement. Thus, the bubble movement in magnetic nanofluid is numerically investigated for effective energy generation. Slug characteristics are also investigated because a slug can be generated by the merging of bubbles. The level-set method and phase-field method are used to investigate the bubble and slug movements, respectively. For the investigation, EFH1 and EFH3 are selected as working fluids; they are commercial magnetic fluids manufactured by Ferrotec, and EFH3 contains a greater amount of magnetic particles than EFH1. Additionally, the numerical solver is validated by comparing the results with previous research and experimental data. It is confirmed by the validation that the solver can give good results for bubble and slug investigation.

Conclusions of the bubble investigation

- The amount of solid particles can affect the bubble movement because the properties of the fluid are changed by the solid particles. The bubble in EFH1 can move more actively than that in EFH3 because the viscosity of EFH3 is higher than that of EFH1 due to the friction of the additional solid particles.

- When two of bubbles of the same size move in the system, they can move in 4 patterns according to the initial distance between each bubble.

- A large bubble is more effective than small bubbles for energy generation because it can disturb the surrounding magnetic fluid more actively.

Conclusions of the slug investigation

- The amount of solid particles can also affect the slug characteristics because of the property differences. The slug in EFH3 is slower and more stretched than in EFH1 because the higher-viscosity friction is acting on the slug. The wake of the slug in EFH3 is smaller than that in EFH1 because of the higher kinematic viscosity.

- If the slug is long enough, the rising velocity of the slug is not affected by slug length because the drag force is balanced with the acceleration force.

- When the liquid flows downward, the slug's rising velocity and the size of the recirculation flow are decreasing according to the increasing of the liquid velocity. Thus, the rising motion of the slug is more important than the liquid flow for generating the recirculation flow.

- When two slugs are moving in the system, the rear slug is gradually accelerated and moves towards the front slug, and the two slugs are finally merged with each other because the relatively small drag force is acting on the rear slug. Two slugs can interact in just this one pattern because the slug can only move along the fluid domain.

- The merging of slugs can be effective for energy generation because it can induce the active magnetic fluid movement.

Conclusions of the magnetic force investigation

- The bubble can be driven by only the magnetic force. Its direction is determined by the magnetic properties of each fluid and the magnetic field distribution.

- When normal gravity is applied to the system, the magnetic force cannot affect the bubble and slug characteristics because the gravitational force is much greater than the magnetic force.

- For electrical energy generation, the important factor for magnetic fluid disturbance is not the magnetic force but the hydrodynamic force.

References

[1]   D.Bhaga and M. E. Weber, Bubbles in viscous liquids : shapes, wakes and velocities, J. FluidMech (1981), vol. 105, pp. 61-85.

[2]   C. W. Stewart, Bubble interaction in low-viscosity liquid, Int. J. Multiphase Flow (1995) vol. 21, No. 6, pp. 1037-1046

[3]   K. Tsuchiya, K. Ohaki and K. Tanguchi, Large and small bubble interaction patterns in a bubble column, Int. J. Multiphase Flow (1996) vol. 22, No. 1, pp. 121-132.

[4]   R. Krishna and J. M. van Baten, Rise characteristics of gas bubble in a 2D rectangular column : VOF simulation VS Experiments, Int. Comm. Heat Mass Transfer (1999), vol. 26, No. 7, pp. 965-974.

[5]   Zongyuan Xiao and Reginald B. H. Tan, A model for bubble-bubble and bubble-wall interaction in bubble formation, AIChE(American Institute of Chemical Engineers) Journal (2005), vol. 52, No. 1, pp. 86-98

[6]   A. Perron, L. I. Kiss and S. Poncsak, An Experimental investigation of the motion of single bubbles under a slightly inclined surface, International Journal of Multiphase Flow 32 (2006), pp. 606-622.

[7]   Alexander Zaruba, Dirk Lucas, Horst-Michael Prasser and Thomas Hohne, Bubble-wall interactions in a vertical gas-liquid flow : Bouncing, sliding and bubble deformations, Chemical Engineering Science 62 (2007), pp. 1591-1605.

[8]   Zhao Yu and Liang-Shih Fan, Direct simulation of the buoyant rise of bubbles in infinite liquid using level set method, The Canadian Journal Of Chemical Engineering (2008), vol. 86, pp. 267-275.

[9]   Toshiyki Sanada, Ayaka Sato, Minori Shirota and Masao Watanabe, Motion and Coalescence of a bubbles rising side by side, Chemical Engineering Science 64 (2009), pp. 1191-1207.

[10]   K. Dilleswara Rao, M. Vasukiran, A. R. K. Gollakota and Nanda Kishore, Buoyancy driven bubble rise and deformation in milli/micro channels filled with shear-thinning nanofluids, Colloids and Surface A : physicoschem Eng. Aspects 467 (2015), pp. 66-77

[11]   H. L. Goldsmith and S. G. Mason, The movement of single large bubbles in closed vertical tubes, Journal of Fluid Mechanics (1962), vol. 14, pp. 42-58.

[12]   E. T. White and R. H. Beardmore, The velocity of rise of single cylindrical air bubbles through liquids contained in vertical tubes, Chemical Engineering Science (1962), vol. 17, pp. 351-361.

[13]   J. B. L. M. Campos and J. R. F. Guedes De Carvalho, An experimental study of the wake of gas slugs rising in liquids, J. Fluid Mech. (1988), vol. 196, pp. 27-37.

[14]   Taha Taha, Z. F. Cui, CFD modelling of slug flow in vertical tubes, Chemical Engineering Science 61 (2006), 676-687.

[15]   H. C. Brinkman, The viscosity of concentrated suspensions and solutions, The journal of chemical physics (1951), vol. 20, No. 4, pp. 571.

[16]   S. M. Sohel Murshed and Nam-Trung Nguyen, Characterization of temperature dependence of interfacial tension and viscosity of nanofluid, Micro/Nanoscale Heat transfer international conference, January 6-9, 2008, Tainan, Taiwan.

[17]   Saad Tanvir and Li Qiao, Surface tension of nanofluid-type fuels containing suspended nanomaterials, Nanoscale Research Letters (2012), 7:226.

[18]   N. I. Wakayama, H. Ito, Y. Kuroda, O. Fujita and K. Ito, Magnetic support of combustion in

diffusion flames under microgravity, Elsevier Science Inc, Combustion and Flame 107 : 187-192 (1996).

[19]   Nobuko I. Wakayama, Magnetic buoyancy force acting on bubbles in nonconducting and diamagnetic fluids under microgravity, J. Appl. Phys. (1997), vol. 81, No. 7, pp. 2980-2984.

[20]   Jianwei Qi, Nobuko I. Wakayama and Akira Yabe, Magnetic control of thermal convection in electrically non-conducting or low-conducting paramagnetic fluids, International Journal of Heat and Mass Transfer 44 (2001), pp. 3043-3052.

[21]   L. B. Wang and Nobuko I. Wakayama, Control of natural convection in non- and low-conducting diamagnetic fluids in a cubical enclosure using inhomogeneous magnetic fields with different directions, Chemical Engineering Science 57 (2002), pp. 1867-1876.

[22]   Nobuko I. Wakayama, Chengwen Zhong, Tsukasa Kiyoshi, Kikuo Itoh and Hitoshi Wada, Control of vertical acceleration (Effective gravity) between normal and micro gravity, AIChE Journal, vol. 37, No. 12, pp. 2640-2643.

[23]   Ion Iliuta and Faical Larachi, Modelling and simulation of trickle-bed magnetohydrodynamics in inhomogeneous magnetic fields, Chemical Engineering and Processing 45 (2004), pp. 1417-1427.

[24]   Customer model library, COMSOL Multiphysics ver. 4.2a.

Acknowledgements

I would like to express my deep gratitude for my advisor Professor Jaeseon Lee. This study would not have been possible without his guidance and persistent help. I am honored that I could study under Professor Jaeseon Lee.

I would also like to thank my committee members; Professor Chun Sang Yoo and Professor Jae Hwa Lee. It would be difficult to finish the study without their useful comments.

I would like to thank my laboratory members. This study would not been completed without their advice and assistance.

Lastly, I would like to express my sincerest thanks to my family for their moral and financial support in order to finish this study.

Dongkook Joo